The role of groundwater in the Amazon water cycle: 2. Influence on seasonal soil moisture and evapotranspiration

Gonzalo Miguez-Macho[1] and Ying Fan[2]

Received 30 January 2012; revised 29 June 2012; accepted 2 July 2012; published 14 August 2012.

[1] We investigate the potential influence of groundwater on seasonal evapotranspiration (ET) in the Amazon using a coupled groundwater-surface water model (LEAF-Hydro-Flood) forced with ERA-Interim reanalysis, at 2 km grid and 4 min steps over 11 yrs (2000–2010), and validated with available soil moisture and ET observations. We find that first, the simulated water table is <2 m deep over a significant portion of the Amazon (20–40%). Second, shallow groundwater can reduce wet season soil drainage, leading to larger soil water stores before the dry season arrives. Third, capillary rises from the water table can reach the root zone and maintain high dry season ET near the valleys. Fourth, groundwater's delayed response to rainfall can buffer surface stress in the dry season, when groundwater is the shallowest. Fifth, this temporal delay can be seen as spatial patterns; continued drainage and convergence maintain moist valleys forming a structured mosaic of wet-dry patches in the dry season. Results from two parallel runs, with and without groundwater, suggest that overall groundwater made a large difference in modeled soil moisture where the water table is shallow, but it only made a difference in modeled ET where the seasonality is strong; over southeastern Amazonia, July–August ET differs by ~1 mm/day. We note that our results are based on model simulations, which only suggest the potential importance of the groundwater system to the Amazon water cycle. The ultimate knowledge must come from carefully designed field observations linking vegetation, soil and groundwater with water balance studies and tracer tests, across a range of physical-biological settings.

Citation: Miguez-Macho, G., and Y. Fan (2012), The role of groundwater in the Amazon water cycle: 2. Influence on seasonal soil moisture and evapotranspiration, *J. Geophys. Res.*, *117*, D15114, doi:10.1029/2012JD017540.

1. Introduction

[2] This is the second of a two-part series investigating groundwater's influence on the Amazon water cycle. In the first part [*Miguez-Macho and Fan*, 2012] we focused on the groundwater's role in seasonal river discharge, floodplain inundation and wetlands using a continental-scale, high-resolution land model that mechanistically couples the groundwater, surface water and soil moisture stores. We find that the groundwater can regulate surface water dynamics through several mechanisms. First, in the small catchments across the Amazon, steady groundwater drainage and convergence can support the bulk of streamflow all year-round, and the groundwater contribution is likely greater where the water table is deeper (limiting saturation-overland runoff). Second, over the floodplains, the two-way exchange between floodwater and groundwater can be controlled by the shallow water table (limiting infiltration loss in wet season and feeding swamps in dry season). Third, groundwater can support large wetlands rarely flooded but characterized with a shallow water table. Fourth, the delayed and muted subsurface response to rainfall can cause groundwater seepage to persist in the dry season, buffering rivers and wetlands during seasonal droughts. In this second part, we focus on potential groundwater influence on seasonal soil moisture and evapotranspiration (ET).

[3] The Amazon harbors the largest and richest tropical forest stand on the planet. To understand the impact of deforestation and potential climate change on its well-being requires a mechanistic understanding of its responses and feedbacks to changes in its physical environment. One question is how well the forest fares in the dry season and droughts under today's climate, which is pertinent to projecting how well it may fare under a future climate with a likely longer dry season [*Malhi et al.*, 2009; *Poulter et al.*, 2010; *Marengo et al.*, 2011; *Good et al.*, 2011; *Zelazowski et al.*, 2011]. Although annual rainfall is abundant, large regions of the Amazon experience a multimonth dry season; the seasonal migration of the Inter-Tropical Convergence Zone (ITCZ) over the Amazon leads to pronounced seasonality in rainfall and distinct seasonal swings in soil moisture, river flow and flooding. Soil water stress and reduced photosynthesis are

[1]Nonlinear Physics Group, Faculty of Physics 15782, Universidade de Santiago de Compostela, Galicia, Spain.
[2]Department of Earth and Planetary Sciences, Rutgers, State University of New Jersey, New Brunswick, New Jersey, USA.

Corresponding author: Y. Fan, Department of Earth and Planetary Sciences, Rutgers, State University of New Jersey, New Brunswick, NJ 08854, USA. (yingfan@rci.rutgers.edu)

©2012. American Geophysical Union. All Rights Reserved.
0148-0227/12/2012JD017540

indeed suggested by current climate and ecosystem models [e.g., *Kleidon and Heimann*, 2000; *Werth and Avissar*, 2004; *Baker et al.*, 2008; *da Rocha et al.*, 2009; *Verbeeck et al.*, 2011], although a seminal paper two decades ago [*Shuttleworth*, 1988], based on observations and model syntheses, had shown that ET in the dry season is no less than in the wet season in an evergreen forest in the central Amazon. Recent flux measurements at multiple sites and satellite images revealed similar findings [*Saleska et al.*, 2003; *da Rocha et al.*, 2004; *Goulden et al.*, 2004; *Xiao et al.*, 2005; *Bruno et al.*, 2006; *Huete et al.*, 2006; *Ichii et al.*, 2007; *Myneni et al.*, 2007; *Juárez et al.*, 2007; *Fisher et al.*, 2009; *Saleska et al.*, 2009; *Verbeeck et al.*, 2011], all suggesting that the Amazon forest as a whole does well in the dry season. Recent syntheses of flux tower observations across the Amazon [*Juárez et al.*, 2007; *da Rocha et al.*, 2009] and the whole tropics [*Fisher et al.*, 2009] further confirmed that net radiation is the primary driver of seasonal ET, pointing to a general absence of water stress contrary to what is suggested by models.

[4] A rich body of literature can be found proposing different mechanisms to explain this observation-model discrepancy. First, it is widely acknowledged that soil water store in nature can be far greater than assumed in models which have a typical soil column of 2–3 m in depth; in nature, the deeper soil store is filled in the wet season and can help support ET in the following dry season; in models, excess infiltration drains freely through the shallow soil column and is removed as river outflow, no longer available for plant use later.

[5] Second, it is recognized that tree roots can extend far deeper than model rooting depth and can access deep stores [*Nepstad et al.*, 1994; *Kleidon and Heimann*, 2000; *Ichii et al.*, 2007; *Grant et al.*, 2009; *Harper et al.*, 2010; *Markewitz et al.*, 2010; *Verbeeck et al.*, 2011]. However, global syntheses of rooting-depth measurements suggest that 95% of root mass resides in the top 2 m soil for all major biomes [*Schenk and Jackson*, 2002], and tracer studies in the Amazon suggest that direct root uptake does not seem to occur beyond the 2 m depth [*Sternberg et al.*, 2002; *Romero-Saltos et al.*, 2005]. (We note that 'direct root uptake' is not the same as 'soil water depletion'; the latter can be caused by downward gravity drainage, upward or downward capillary flux, as well as direct root uptake. Carefully designed tracer tests can pinpoint roots as the direct soil water sink as in *Moreira et al.* [2000], *Sternberg et al.* [2002] and *Romero-Saltos et al.* [2005], further discussed later). The observations that roots tend to occupy shallow soils, and that they do not directly harvest water at greater depths, indicate uncertainty regarding the functions of deep roots [*Schulze et al.*, 1996; *Moreira et al.*, 2000] and seem to justify the commonly used 2–3 m soil depth in models.

[6] Third, the small fraction of deep roots can be water conduits via hydraulic redistribution (HR) whereby soil water is transported through roots from wet to dry soils [*Dawson*, 1993; *Caldwell et al.*, 1998; *Burgess et al.*, 1998; *Amenu and Kumar*, 2008]. Nighttime sap flow in tap-root xylems has been detected in Amazon species [*Oliveira et al.*, 2005], and roots were found at 18 m depth [*Nepstad et al.*, 1994]. Global synthesis suggests that roots can indeed reach tens of meters in plants relying on deep sources in an arid climate [*Canadell et al.*, 1996]. A model study [*Lee et al.*, 2005] found that incorporating HR assuming its occurrence in all species significantly reduced, although far from eliminated, the model ET bias. Another modeling study [*Baker et al.*, 2008] further shows that the combination of all the above (deep soil, deep roots, HR) performs better than any single one alone. A recent model evaluation of HR in the Amazon [*Wang*, 2011] suggests that it enhances dry season ET in general but can also deplete deep stores too early in the dry season.

[7] Fourth, tracer tests and soil water budget studies revealed evidence of upward soil water flux driven by capillary tension, from the deeper-wetter soil to the shallower-drier soil in the dry season [e.g., *da Rocha et al.*, 2004; *Romero-Saltos et al.*, 2005; *Bruno et al.*, 2006; *Borma et al.*, 2009]. The most instructive is the deuterium tracer pulse-chase study of *Romero-Saltos et al.* [2005] near Santarem, where deuterium-enriched water was sprinkled on soil surface, and deuterium label was 'chased' down the soil profile and up the stem xylems in separate wet and dry season experiments. In the wet season experiment, deuterium label is found in stems when the pulse is in the top 2 m soil, accompanied by substantial deuterium loss from the soil, but the label in stems disappeared after the pulse has infiltrated below 2 m depth with no further deuterium loss. In the dry season experiment, the pulse moved up the soil by ~64 cm in four months and the label reappeared in the stem as the pulse rose to above 2 m depth. Careful interpretation of the pulse shape ruled out HR as the cause and pointed to soil capillary flux [*Romero-Saltos et al.*, 2005]. Together, the two seasonal experiments suggest that first, roots did not take up water below 2 m depth, and second, the upward capillary flux made this possible by pumping deeper water to the shallower root zone. Capillary flux is known to be significant in fine-textured soils because of larger particle surface area and narrower pores [e.g., *Freeze and Cherry*, 1979]. Soils in the Amazon are dominated by deeply weathered Oxisols with high clay contents, which can potentially render capillary flux an important physical process of soil water transport.

[8] Fifth and lastly, a water table fluctuating near the root zone can be a direct source for roots. Diurnal variations in water table depth in a Suriname rain forest are indications of direct water table contribution to forest ET [*Poels*, 1987]. Scattered field observations across the Amazon suggest ubiquitously shallow water table (<2 m) near the valley floors and 5–40 m deep under high grounds (*Brazilian Geological Survey* as compiled in *Fan and Miguez-Macho* [2010]; *Bongers et al.* [1985]; *Poels* [1987]; *Lesack* [1995]; *Coomes and Grubb* [1996]; *Hodnett et al.* [1997a], [1997b]; *McClain et al.* [1997]; *Selhorst et al.* [2003]; *Grogan and Galvão* [2006]; *Jirka et al.* [2007]; *Tomasella et al.* [2008]; *Cuartas* [2008]; *Vourlitis et al.* [2008]; *Borma et al.* [2009]; *Lähteenoja and Page* [2011]; and *Neu et al.* [2011]). Given the possible range of rooting depths in the Amazon tree species, it is plausible that some may directly tap the groundwater.

[9] In this study, we propose that the groundwater reservoir under the Amazon may help explain the observed absence of dry season water stress, because it is related directly or indirectly to all the above mechanisms. If the water table resides in the top 2–3 m, then it increases soil water store (mechanism 1, 2) and provides for direct root uptake (mechanism 5); if the water table is below the top 2–3 m but within the reach of deep tap roots (3–15 m), then it enhances

HR (mechanism 3) by providing a deep source and supplies capillary rise (mechanism 4) in fine textured soils. Observations suggest that the water table can be sufficiently shallow under portions of the Amazon as to be relevant to these mechanisms. But its potential contribution has not been systematically examined across different hydrologic-ecologic settings of the Amazon; scattered water table observations suggest common occurrence of shallow groundwater, but except for *Vourlitis et al.* [2008] and *Borma et al.* [2009], there are no simultaneous soil moisture measurements to allow integrated analyses; similarly, soil moisture monitoring and tracer tests (*da Rocha et al.* [2004], *Romero-Saltos et al.* [2005], *Bruno et al.* [2006], and others) inferred upward soil capillary flux in the dry season, but the monitoring did not reach the water table as to identify the ultimate source, locally wet soil versus groundwater. In addition, these observations are only a small sample of the vast Amazon ecosystem.

[10] In the absence of sufficient and integrated observations necessary for a comprehensive understanding of groundwater contribution to seasonal ET across the Amazon, a modeling study may provide a framework for synthesis and comparisons across scattered field sites. It can also shed lights on the mechanistic links between soil moisture and groundwater stores and the implications to ET and photosynthesis. To do so, the model must realistically represent the dynamic groundwater-soil water exchange at scales meaningful to land hydrology, demanding the following capabilities. First, it must include a prognostic groundwater store with two-way exchange with the soil water, rivers, floodplains and wetlands governed by the hydraulic gradient between each pair of stores. Second, the model must resolve the difference between hilltops and river valleys because surface runoff and groundwater convergence are most pronounced at this scale; It is widely and intuitively understood that the valleys are moister than hilltops, particularly in dry periods, due to hill-to-valley convergence; this moisture gradient also frequently manifests itself into soil and vegetation gradients and hence it is a meaningful and fundamental scale for surface processes. To capture this scale requires a model grid size of tens of meters to a few kilometers, a computational challenge for continental scale models but nonetheless needs to be met to the extent feasible. Third, the model should encompass the large spatial variability across the Amazon to allow comparisons and syntheses of process controls across regimes within the same modeling framework, calling for continental-scale model domains. Fourth, the model must be validated by available observations in key reservoirs at key scales so that the dynamics are correctly represented at catchment to basin, and event to seasonal and inter-annual scales. This implies that the available observations must be used for constraining model performance at point (soil moisture, water table depth), plot (eddy-covariance tower fluxes, throughfall experiments) and basin (streamflow, flooding) scales.

[11] To our knowledge such a modeling exercise in the Amazon has not been completed. Global simulations incorporating the water table [e.g., *Niu et al.*, 2007; *Lo and Famiglietti*, 2010, 2011; *Niu et al.*, 2011; *Yang et al.*, 2011; *Good et al.*, 2011] could not resolve local convergence fundamental to land hydrology and the maintenance of wet valleys. With a large model grid size, validations with observations of water table, soil moisture and tower fluxes are difficult and hence seldom performed, leaving doubts in model realism. Our preliminary work [*Fan and Miguez-Macho*, 2010] estimated the potential (maximum) upward capillary flux from the water table at the hill-valley scale (9 arc-second grid, ~270 m), but it assumed hydrologic equilibrium which does not shed lights on seasonal dynamics essential to the Amazon. To satisfy the model requirements outlined above and to overcome the deficiencies in current global models, we developed LEAF-Hydro-Flood, an integrated groundwater-surface water, high-resolution and continental-scale land hydrology model, and apply it here to assess the functions of the groundwater in Amazon seasonal soil moisture and ET dynamics. The model will be described in detail in the next section.

[12] Using this model, we will investigate the potential importance of the following mechanisms. First, a shallow water table can be a direct source for plant uptake as schematically illustrated in Figure 1a where a hill-valley cross-section is shown as model columns. If the water table is indeed shallow under the valleys and floodplains as observations suggest, trees growing near the valley can directly tap the water table. The extensive wetlands and flooded forests in the central Amazon may directly utilize the shallow groundwater. Second, where the water table is shallow, drainage in the wet season can be reduced; impeded drainage is intuitively associated with swampy conditions such as in tropical lowlands and coastal valleys. Observations and a model synthesis [*Miguez-Macho and Fan*, 2012, Figure 1] suggest that shallow water table conditions occur under large regions of the Amazon such as in the Andean foreland basins and river valleys elsewhere, and thus it is conceivable that a significant portion of the Amazon does not drain efficiently in the wet season. As illustrated in Figure 1b, a typical, fixed-depth, model soil column (red) with free drainage at the base may describe the hilltop well (soil column above water table) but will artificially accelerate drainage near the valleys. Drainage is relevant because reduced drainage loss in the wet season leads to a larger soil water store at the beginning of the dry season, giving the Amazon forest a strong start. Third, where the water table is sufficiently shallow, capillary rise from the water table can reach the root zone, as illustrated in Figure 1c. It is possible that during day time, ET and root uptake outpaces capillary supply, resulting in the observed soil water depletion in the root-zone; during nighttime, root uptake halts and capillary supply replenishes the root zone, resulting in the observed nighttime soil water recovery. Capillary rise is only centimeters in sandy soils but can reach tens of meters in silt and clay soils [e.g., *Freeze and Cherry*, 1979], and clay is common in the deeply weathered Amazon. Fourth and lastly, due to its delayed and dampened response to seasonal rainfall, the timing of groundwater can potentially buffer dry season surface stress (see discussion in *Eltahir and Yeh* [1999]). Across the Amazon, it has been shown that the water table reaches its seasonal peak weeks to months after the peak seasonal rainfall [*Hodnett et al.*, 1997a, 1997b; *Johnson et al.*, 2006; *Grogan and Galvão*, 2006; *Cuartas*, 2008; *Vourlitis et al.*, 2008; *Tomasella et al.*, 2008], and the surplus or deficit in groundwater stores from one season can carry over to the next [*Tomasella et al.*, 2008]. This is schematically illustrated in Figure 1d with a hypothetical seasonal rainfall and water table depth below the hilltop and the valley. Below the high grounds, the water table is deeper

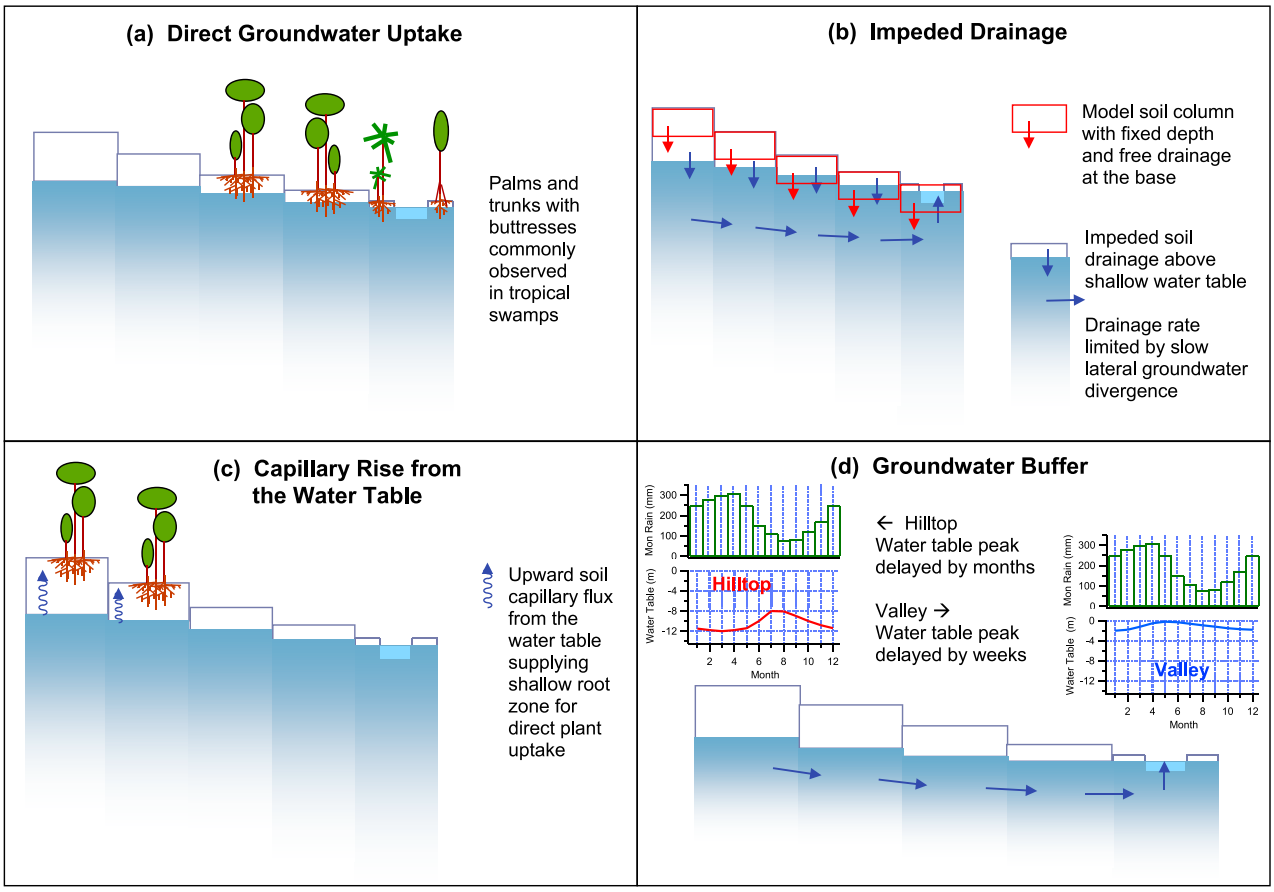

Figure 1. Schematic illustrations of the four hypotheses tested in this study.

with longer delayed response to seasonal rainfall; near the valleys, the water table is shallower with shorter delayed response. This can cause the groundwater to be the shallowest when the surface begins to dry, maximizing its influence on the surface as a source from below. The temporal delay may also manifest itself as spatial patterns; throughout the dry season, continued drainage and convergence can sustain a shallow water table in the lowlands, keeping them moist all year-round and forming a structured mosaic of wet-dry patches in the dry season, supporting ET at least in the lower parts of the landscape.

[13] We test the relevance of these mechanisms in the Amazon using LEAF-Hydro-Flood, validated in the companion paper with observed river discharge, seasonal flooding, water table depth, and further validated here with observed soil moisture and ET flux. Most of the observations are outcomes of the Large-scale Atmosphere-Biosphere Experiment in the Amazon (LBA), a Brazil-led international effort to understand the biogeochemical functioning of the Amazon ecosystem and its future under multiple threats. Through systematic observations (e.g., the network of eddy-covariance flux towers) and synthesis efforts of LBA, the scientific community has gained tremendous insight into the water, energy, carbon, nutrient and trace-gas dynamics across the Amazon (see LBA review volume [*Keller et al.*, 2009]). The observations and syntheses have challenged the models by revealing their departures from observations referenced earlier and underscored the need for improving our models' realism. While there are enormous challenges in realistically representing the carbon and nutrient cycles in the Amazon in land ecosystem models [*Sakaguchi et al.*, 2011], we note that some of the basic physics of land hydrology are still inadequately represented in current models. Some of the long-established hydrologic knowledge, such as groundwater convergence as a spatial organizer and temporal buffer of land surface moisture states, and the dynamic two-way exchange between groundwater and surface waters at a range of scales [e.g., *Winter et al.*, 1998], are still inadequately described in large-scale land hydrology and ecosystem models. In this study we explicitly incorporate such hydrologic common sense into a continental-scale model to assess groundwater's relevance to Amazon land-atmosphere fluxes. The model and simulations are described in section 2, validations in section 3, results and analyses in section 4, a summary in section 5 with discussions on potential implications to the Amazon carbon cycle.

2. Model Description and Simulation Setup

[14] The model we use is called LEAF-Hydro-Flood, schematically shown in Figure 2. Orange color-coding represents the stores and fluxes in standard LEAF (Land-Ecosystem-Atmosphere Feedback), the land model of RAMS (Regional Atmosphere Modeling System), a regional climate model developed at Colorado State University (http://www.atmet.com) and widely applied to climate research. Detailed descriptions of LEAF are given in *Walko*

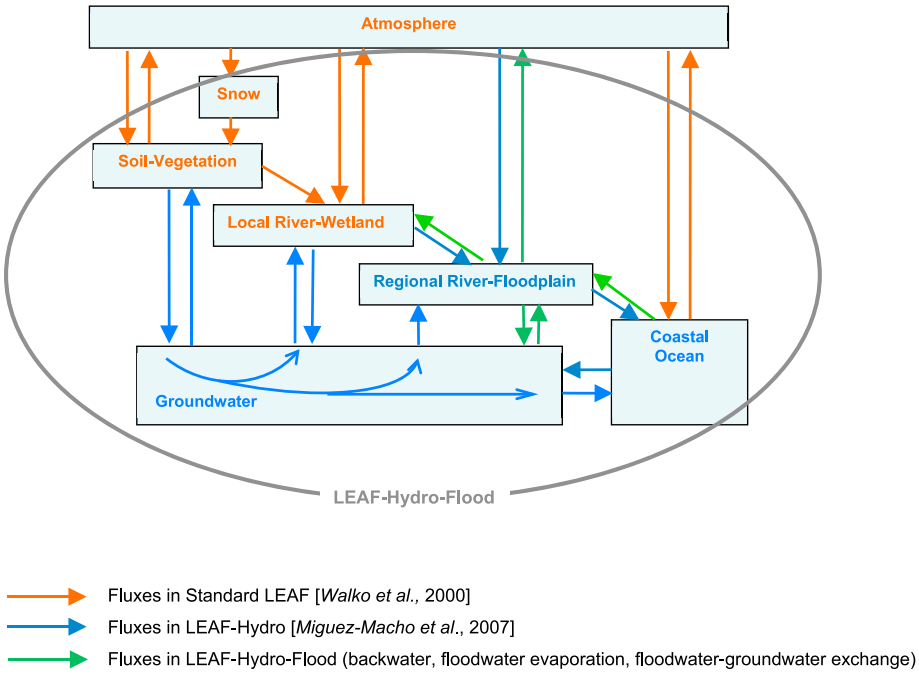

Figure 2. Stores and fluxes included in standard LEAF (orange color-coding) and other typical land models, LEAF-Hydro (blue color-coding), and LEAF-Hydro-Flood (green color-coding).

et al. [2000]; it includes prognostic water-energy in multiple layers in the soil column to a user-defined depth, a surface store (ponding and snow), a vegetation store, and a canopy air store.

[15] Several fundamental changes were made to LEAF through our earlier work over N. America [*Miguez-Macho et al.*, 2007], resulting in LEAF-Hydro (Figure 2, blue color-coding). It centers at the addition of a prognostic groundwater store and two-way exchanges with soil-vegetation, rivers-wetlands within a model cell (local), and rivers-wetlands in down-gradient cells (regional box). Changes in the code include (1) extending the soil column to the dynamic water table below, the latter acting as saturation boundary condition, (2) allowing the water table, once recharged by rain events, to relax through discharge into rivers within the grid cell and lateral groundwater flow to adjacent cells, leading to divergence from high grounds and convergence in low valleys at a range of scales resolved by the model, (3) allowing two-way exchange between groundwater and rivers depending on their water level gradient, representing both loosing (leaking to groundwater) and gaining (receiving groundwater) streams, (4) routing the rivers, receiving surface runoff and groundwater convergence, to the ocean through the channel network, and (5) setting the sea level as the groundwater head boundary condition, hence allowing sea level to control coastal drainage.

[16] In applying the model to the Amazon, we (6) further introduced a new river-floodplain routing scheme that solves the full momentum equation of open channel flow, taking into account the backwater effect (the diffusion term) and the inertia of large water mass in deep flow (the acceleration terms), both recognized as important in the Amazon river system [e.g., *Meade et al.*, 1991; *Trigg et al.*, 2009]. The full momentum equation is solved in river channels and over floodplains with semi-explicit finite difference code that is computationally efficient and stable, following the guidance of *Bates et al.* [2010] and *Yamazaki et al.* [2011] using a Runge-Kutta method to increase time step length of integration [*Press et al.*, 1989]. The simulated streamflow correctly reflects the floodplain storage effect and the simulated seasonal flooding compares very well with satellite observations. Due to the large area covered by seasonal flooding in the Amazon, we (7) enable direct evaporation from floodwater and (8) enable direct floodplain-groundwater exchange by allowing floodwater infiltration and groundwater seepage, determined by relative water surface elevation. Groundwater seepage has been widely documented on the Amazon floodplains [e.g., *Forsberg et al.*, 1988; *Lesack*, 1995; *Lesack and Melack*, 1995; *Mertes*, 1997; *Cullmann et al.*, 2006; *Hamilton et al.*, 2007; *Bonnet et al.*, 2008; *Bourrel et al.*, 2009; *Borma et al.*, 2009] and it is thought to support the back swamps and floodplain lakes in the dry season. To differentiate from the earlier version, we refer to the model here, with its newly added backwater floodplain processes, as LEAF-Hydro-Flood, as represented by the green arrows in Figure 2. Details of the new model components are given in the companion paper. Below, we only describe the recent and minor changes in the evapotranspiration scheme to improve the partition of total ET into interception, plant transpiration, and surface evaporation.

2.1. Improving ET Partitioning

[17] Of the three components, only canopy interception is directly inferred from forest throughfall and stemflow measurements. A literature compilation by *Dingman* [2002] gives a range from 5% (tropical evergreens) to 49% (conifers) of total annual rainfall. Recent reviews by *Wang et al.* [2007] and *Czikowsky and Fitzjarrald* [2009] report site

values in the tropics ranging 4% to 37%. Since interception depends on rainfall intensity, large variations are expected across seasons and sites. In the central Amazon near Manaus, *Cuartas* [2008], based on 5-min stemflow and throughfall measurements over 2002–2004, report 13.3% in a normal year and 22.6% in a drier year, and 13.9% to 21.4% in the wet season and 12.0% to 25.0% in the dry season. In the eastern Amazon near Santarem, *Czikowsky and Fitzjarrald* [2009], based on a new method using eddy-covariance flux measurements over 2001–2003, report 10% for moderate rain-rate daytime events, 18% for light events, and 7.8% for heavy events, with the mean for all daytime and nocturnal events of 11.6%. These values, based on the respective ET estimates at the two locations, translate into about 1/3 of total ET near Manaus [*Cuartas*, 2008] and 1/5 near Santarem [*Czikowsky and Fitzjarrald*, 2009].

[18] Compared to these values, interception from standard LEAF is much higher at the same locations, accounting for 80% of total ET in the wet season near Santarem with near complete shutdown in transpiration. Over-estimating interception loss appears common among global land models, for reasons from the much reduced storm intensity when averaged over large grid cells and/or multihour time steps [e.g., *Eltahir and Bras*, 1993; *Wang and Eltahir*, 2000], to parameterizations of interception [*Wang et al.*, 2007] and transpiration during events [e.g., *Lawrence et al.*, 2007]. Here, we take the following steps to reduce the large positive bias.

[19] First, we concentrate the 3-hourly rainfall forcing into shorter periods based on observed duration-depth relations. Figure 3a is the distribution of rainfall duration from 3,376 3-h periods that report rainfall, based on 30-min observations at an LBA site near Santarem (data courtesy of LBA Data-Model-Intercomparison Project (L. G. G. de Goncalves *et al.*, Overview of the Large-Scale Biosphere-Atmosphere Experiment in Amazônia Data Model Intercomparison Project (LBA-DMIP), submitted to *Agricultural and Forest Meteorology*, 2012). Half of the samples received the 3-h rain within 30 min. The empirical relation between the duration and the total rainfall amount in a 3-h period is shown in Figure 3b. The 1-stardard deviation bars suggest large scatter, but the mean is highly correlated with total rainfall (Pearson correlation coefficient 0.99). The same analyses were performed with observations at other LBA sites with similar results (not shown), although most of the sites have only hourly data (versus 30-min at Santarem). The relationship shown in Figure 3b is used here. Second, we allow partial transpiration during rain events. In standard LEAF, the fraction of leaf area that can transpire depends on canopy storage (zero at full storage). In tropical forests stomata are found only on the underside of leaves in over 95% of the species [*Grubb*, 1977], and plants continue to transpire as the top is wetted. We allow 75% of the leaf area to transpire at full canopy storage, similar to the recent modification in the Community Land Model (CLM) by *Lawrence et al.* [2007]. Third, we allow diffuse radiation to reach the lower part of the canopy so that transpiration can occur in partial shade, following *Thornton and Zimmerman* [2007] and *Lawrence et al.* [2007]. Finally, a surface litter resistance is introduced into LEAF, also following CLM [*Sakaguchi and Zeng*, 2009], in calculating evaporation from the forest floor, which reduced bare soil evaporation. These modifications are based on improved understanding of biophysics reported and tested in recent modeling literature, and no parameters are tuned to achieve the desired ET partitioning once these changes are made.

2.2. Land Surface Parameters

[20] The companion paper has provided detailed descriptions of the digital land-surface elevation data, river network delineation, and the calculation of river-floodplain hydraulic parameters. Of particularly importance to this study, regarding land surface fluxes, are soil, land cover, and vegetation biophysical parameters. Land-cover data is obtained from Global Land Cover 2000 Product by the European Commission Joint Research Center (http://bioval.jrc.ec.europa.eu/products/glc2000/products.php). The S. America map, at 1 km grids, is produced from four sets of satellite data [*Eva et al.*, 2004], each better suited to detect certain land surface attributes, and it represents the most recent and complete data set of such.

[21] Soil data is obtained from UNESCO's Food and Agriculture Organization (FAO) digital soil map of the world at 5 arc-minute grids (http://www.fao.org/nr/land/soils/digital-soil-map-of-the-world/en/). Fractions of silt, clay, and sand are mapped into 12 texture classes as defined by the U.S. Department of Agriculture (http://soils.usda.gov/education/resources/lessons/texture/). A map of the 12 texture classes is shown in Figure 4a; the dominant soil types in the Amazon are clay-loam (class 8) and clay (class 11). LEAF assigns soil hydraulic parameters to the 12 classes based on BATS (Biosphere-atmosphere transfer scheme [*Dickinson et al.*, 1986]) using the pedo-transfer function of *Clapp and Hornberger* [1978]. Soil layer configuration is shown in Figure 4b; layer thickness increases downward (5, 5, 10, 10, 10, 20, 20, 20, 50, 50, 50, 50, 50, 50 cm) for the top 4.0 m which are solved with Richards Equation. If the water table is within 4 m (Figure 4b, Water Table 1) soil flux is calculated above it with saturation at the water table, and if the water table is below 4 m (Figure 4b, Water Table 2) a variable thickness layer is added extending the soil column to the water table [*Miguez-Macho et al.*, 2007].

[22] The 30 land cover classes and vegetation biophysical parameters in LEAF are described in *Walko and Tremback* [2005], largely based on SiB2 global land parameter data set of *Sellers et al.* [1996a, 1996b]. Plant rooting depth ranges from 0.7 m for grass-crop to 1.2 m for broadleaf forests. With our soil layer configuration (Figure 4b), roots can directly draw soil water above 1.5 m depth. Given the recent debate on deep root functions in the Amazon, this appears very shallow. But since the focus of the study is groundwater as a potential source for root-zone soil moisture, it is helpful to maintain these standard parameters. Other vegetation parameters, such as leaf area index (LAI) and surface albedo, are monthly values calculated from the NOAA Global Monthly Greeness Fraction Data (http://www.emc.ncep.noaa.gov/mmb/gcp/sfcimg/gfrac/index.html), also following SiB2 [*Sellers et al.*, 1996a, 1996b] as described in *Walko and Tremback* [2005].

2.3. Atmospheric Forcing

[23] LEAF-Hydro-Flood is forced with ECMWF- Reanalysis Interim Product (ERA-Interim) (http://www.ecmwf.int/products/data/archive/descriptions/ei/index.html) covering the

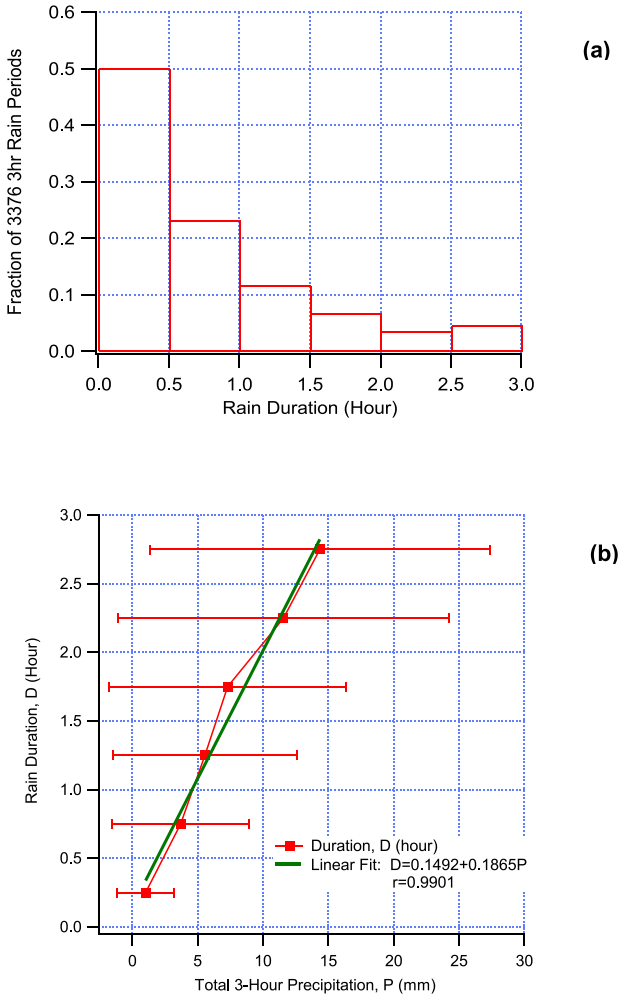

Figure 3. Temporal frequency of rainfall duration if rain is reported within a 3 h period, based on (a) 30-min gage observations of rainfall near Santarem (km77 and km83), and (b) empirical relation between storm duration and total 3-h rainfall amount, based on the same data.

period of 1989-present globally. Analysis was produced daily at 00Z, 06Z, 12Z, and 18Z on a reduced Gaussian grid of N128 (roughly even spacing of ~70 km) for surface fields, and forecasts were produced at 3 hourly steps. Our forcing fields are from the 6 hr analysis for temperature, humidity and wind, and from the 3 hr forecasts for radiation and precipitation to better resolve the event to diurnal changes. A preliminary assessment of ERA-Interim over the Amazon [*Betts et al.*, 2009] suggests significant improvement in annual mean precipitation by removing the drying trend in the earlier product, but seasonal amplitude remains too small and surface air too cool. In the companion paper, we further compared the regional distribution of Interim rainfall with the merged gage-satellite product of GPCP (Global Precipitation Climatology Project [*Adler et al.*, 2003]) [*Miguez-Macho and Fan*, 2012, Figures 6 and 7], which revealed an overall high rainfall bias across the Amazon in addition to the biased-low seasonal amplitude noted by *Betts et al.* [2009].

[24] The product from the South America Land Data Assimilation Project (SALDAS) [*de Goncalves et al.*, 2009] provides an alternative for forcing land hydrology models. It is entirely based on observations, particularly precipitation, from multiple sources and hence offers a potentially improved forcing data set for driving land hydrology, which is highly sensitive to precipitation. However, it only covers the 5 yr period of 2000–2004, too short for studies of interannual variability. The latter, with the role of groundwater as a buffer, is one of the focuses in this study.

[25] Figure 5 plots the monthly precipitation, air temperature, relative humidity, wind speed and downward short and long-wave radiation from ERA-Interim (red), SALDAS (black) and observations (blue) at 5 LBA sites (data courtesy of LBA-Data Model Intercomparison Project (de Goncalves *et al.*, submitted manuscript, 2012) over the period of overlap with our simulation (2000–2010). The small ERA-Interim seasonal amplitude in precipitation, noted by *Betts et al.* [2009] and further shown in the companion paper in different parts of Amazon, is apparent at all sites except Bananal Island. Significant discrepancies in air humidity, wind speed and downward radiation are also apparent at most sites. The SALDAS data set differs from observations significantly in southwestern Amazon (Acre and Jaru) although its precipitation follows the observations more closely. Effects of the ERA-Interim forcing biases on the simulations will be discussed in the validation section.

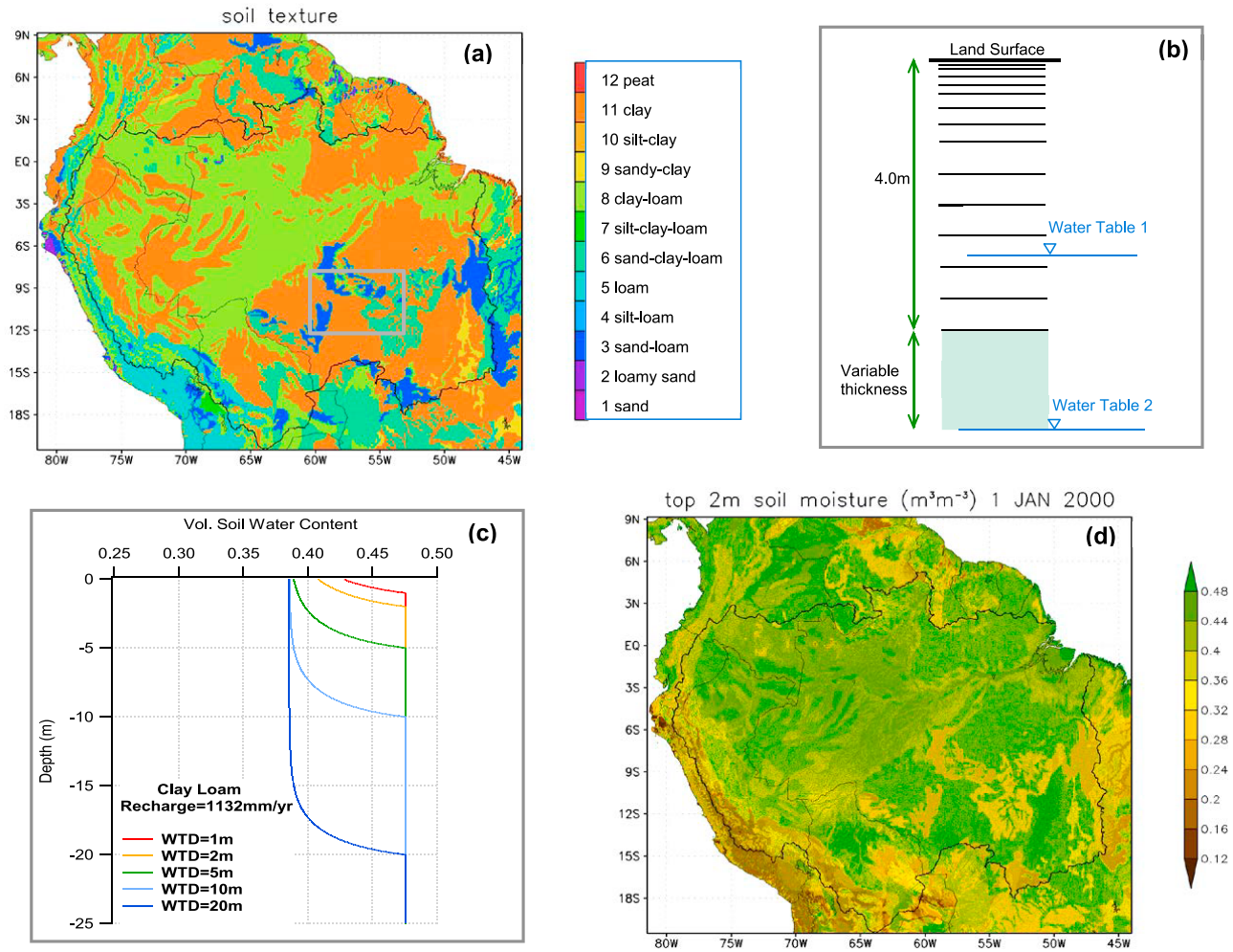

Figure 4. (a) Soil texture classes, (b) soil layer configuration, (c) equilibrium soil moisture profile for clay loam (soil class 8), and (d) initial soil moisture fields in the top-2 m. The boundary of Amazon basin is outlined in both maps. The gray box in Figure 4a is the area for local studies later.

2.4. Initial Conditions and Model Resolutions

[26] The initial water table distribution is obtained by a climatologic equilibrium simulation using a simple 2D groundwater model [*Fan and Miguez-Macho*, 2010]. Briefly, the mean climate input, or groundwater recharge (R), is calculated from annual precipitation (P), ET and surface runoff (SR): $R = P - \mathrm{ET} - \mathrm{SR}$. This climate signal is then redistributed by lateral groundwater convergence from hills to valleys per Darcy's law. We obtained recharge from HTESSEL, the land model of ECMWF [*Balsamo et al.*, 2009], of which the reanalysis product is used here. The equilibrium simulation is performed at 9 arc-second (~270 m) grids and validated statistically with 34,351 well observations [*Fan and Miguez-Macho*, 2010]. The high grid resolution is necessary to define rivers as persistent groundwater seepage sites, and to validate with point observations of water table depth (in wells). The resulting water table depth is shown in Figure 1 of *Miguez-Macho and Fan* [2012].

[27] To obtain the initial water table depth for the dynamic simulation here, we aggregate the 9 arc-second to 60 arc-seconds (~2 km), the grid resolution in this study to feasibly allow dynamic integration over 11 years (2000–2010). For the initial soil moisture fields at different depths, we calculate the equilibrium soil water profile by solving the Richards Equation with the mean recharge (R, last paragraph) as the top boundary, and saturation at the initial water table depth as the bottom boundary. Both boundary conditions reflect the long-term mean hydrologic states. The soil moisture distribution in between is the result of equilibrium adjustment to both boundary conditions. An example of this equilibrium soil moisture profile is shown in Figure 4c for clay-loam, the dominant soil texture class in the Amazon (Figure 4a), at water table depths of 1, 2, 5, 10, and 20 m, using the recharge at a grid cell north of Manaus. Applying this to all grid cells results in the top 2 m soil moisture map shown in Figure 4b. It reflects the spatial patterns in both the water table depth [*Miguez-Macho and Fan*, 2012, Figure 1] and the soil texture classes (all sandy soils, class 9, 6, and 3, stand out as drier patches).

[28] The model domain is the 30 × 40 degree box shown in Figures 4a and 4d. At the model grid resolution of 1 arc-minute (~2 km), there are 2250 × 1780 (4,005,000) grid cells in the domain, a significant challenge to the current computation capabilities. We note that even the 2 km grid resolution, the highest we can feasibly achieve at the present,

Table 1. Published Studies With Soil Moisture Observations Over Our Model Period (2000–2010)

	Site	Longitude, Latitude	Source	Topography Position	Vegetation	Depth Available	Soil Type/ Texture	Porosity, Residual Water Content
1	Asu	−60.2, −2.61	*Cuartas* [2008]	plateau, slope, valley	tropical evergreen forest	plateau - to 4.8 m valley - to 1.4 m	plateau - clay valley - sand	Plateau: BATS clay-loam: 0.476, 0.235; obs max = 0.582 – used as porosity; Valley: BATS sand: 0.33, 0.095; obs max = 0.435, min = 0.025 – both used here instead
2	Tapajos (KM83)	−54.58, −3.01	*Bruno et al.* [2006]	flat upland	dense tropical humid forest	0.15, 0.3, 0.6, 1, 2, 3, 4, 6, 8, 10 m	clay oxisol	Report suggest max as porosity, 0.567; min = 0.384 as residual content, close to clay standard 0.419
3	Caxiuana	−51.46, −1.72	*Fisher et al.* [2009]	terra firma, 15 m above river	lowland rain forest	top 3 m	yellow oxisol, 75–83% sand, laterite at 3–4 m	Given in report for 4 layers; mean used here: 0.4335, 0.07025
4	Jaru	−61.93, −10.08	*Juárez et al.* [2007]	terra firme	terra firme forest	0–1, 1–2, 2–3, 3–3.4 m	med-texture red-yellow podsol on saprolite-weathered granite at 1–4 m	Report mention saturation in deepest layer; all time max and min used here: 0.3375, 0.1325
5	Juruena	−58.5, −10,5	*Jirka et al.* [2007]	palm (flooding), upland forest, campinarana (shrub)	ecoton between tropical rain forest - savanna	top 1 m	ultisols, kaolinitic oxisolls(clay), campinarana on sand	Report mention saturation at Palm, max = 0.490, used as porosity; clay-loam resid. content = 0.268, but obs min = 0.205 – used
6	Bananal Island	−50.15, −9.82	*Borma et al.* [2009]	high ground, seasonal flooding	flooded forest and savanna	0.1, 0.2, 0.5, 1, 1.5, 2 m	hydromorphic sandy soil (Gley humic)	BATS sand: 0.33,0.095; Obs max: 0.83 layer1, too high for soil (likely litter); use max of 0.66 in layer2
7	Sinop	−55.33, −11.41	*Vourlitis et al.* [2008]	terra firme	terra firme semi -deciduous forest	5, 25, 75 cm	quartzarenic neosol (∼90% sand)	Report mention top 1 m all sand; BATS sand: 0.33, 0.095; but obs min = 0.04, used as residual content

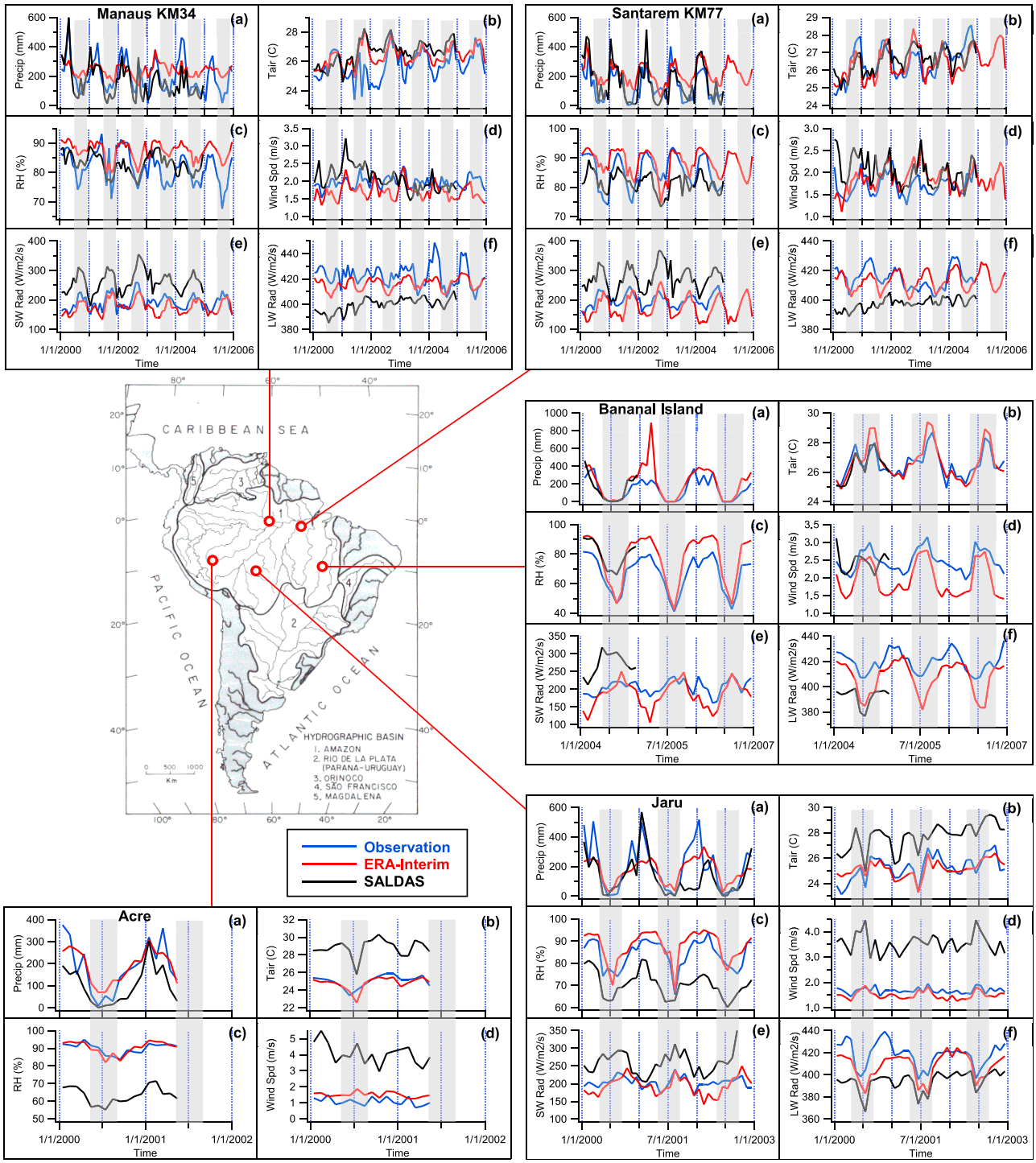

Figure 5. Comparison of (a) monthly precipitation, (b) air temperature, (c) relative humidity, (d) wind speed, (e) short and (f) long wave radiation among ERA-Interim, SALDAS and LBA site observations (dry season shaded).

cannot fully resolve the hill-valley gradient essential to lateral groundwater convergence toward 1st-order streams. However, since the river network and the associated topography are known to exhibit fractal behavior, or similarity in structure across scales (*Rodríguez-Iturbe et al.* [1992]; *Rinaldo et al.* [1992]; *Maritan et al.* [1996]; *Pelletier and Rasmussen* [2009]; among others), the 2 km grid can go a long way to resolve the next higher-order steams (e.g., 2nd and 3rd). It can capture lateral convergence at the local end of the range of scales, a significant refinement from what has been achieved in Amazon basin-scale model studies (e.g., ~10 km in *Coe et al.* [2008], ~15 km in *Beighley et al.* [2009], ~25 km in *Yamazaki et al.* [2011], 1.0 degree in *Poulter et al.* [2010] and *Wang* [2011], 2.8 degree in

Lee et al. [2005], and 2.5 × 3.75 degree in *Good et al.* [2011], etc.). But we caution the reader that our model results at the 2 km grids cannot resolve the hillslopes, and the simulated lateral convergence is best interpreted as from higher-elevation catchments to the lower-elevation valleys of the drainage network.

[29] To reduce computation at this grid resolution, we take advantage of the wide range of time-scales from canopy to groundwater responses, with canopy and soil integrated at 4 min steps, floodplains at 1 min and rivers at 0.5 min where the full momentum equation is solved (for numerical stability, see companion paper), and water table response and lateral groundwater flow at 20 min steps. The computation takes ~12 h to complete a model year using 186 Itanium Montvale processors of the Finis Terrae supercomputer at the CESGA Supercomputer Center of the Universidade de Santiago de Compostela, Galicia, Spain. Model output is saved at daily steps for all variables as limited by data storage.

3. Model Validations

[30] In the companion paper we evaluated the simulations with observed daily streamflow [*Miguez-Macho and Fan*, 2012, Figures 7 and 8] at 10 large gages across the Amazon from Brazilian Agência Nacional de Águas (ANA, http://hidroweb.ana.gov.br/), observed water table depth [*Miguez-Macho and Fan*, 2012, Figure 9] at 8 field study sites reported in the literature [*Selhorst et al.*, 2003; *Germer et al.*, 2010; *Do Nascimento et al.*, 2008; *Cuartas*, 2008; *Jirka et al.*, 2007; *Vourlitis et al.*, 2008; *Grogan and Galvão*, 2006; *Borma et al.*, 2009], and flooding extent [*Miguez-Macho and Fan*, 2012, Figure 10] from high-resolution satellite images and state-of-art image processing tools by *Hess et al.* [2003, 2009]. The results suggest that the model captures the key spatial-temporal features of the Amazon surface and groundwater dynamics. However, the results have an overall wet bias, particularly in the dry season, due to a similar bias in the ERA-Interim rainfall forcing (*Miguez-Macho and Fan* [2012, Figures 6 and 7] and Figure 5). Here, we further validate the simulation with observed soil moisture, ET and interception loss reported in the literature.

[31] We note that no parameters are tuned to match observations. Tuning model parameters would improve model-observation agreement, but since the atmospheric forcing data contains a well-recognized wet bias [*Betts et al.*, 2009], forcing the model to match the observed streamflow would imply an over-estimation of ET, and vice versa. It would be impossible to match both observations if both terms of the water budget closure are evaluated, as they are in this study. By using parameters that are as physically based as possible (e.g., river-floodplain parameters derived from topography only, companion paper), and parameterization widely adopted by the land surface modeling community (e.g., soil and vegetation parameters from SiB2 global land parameter data set, section 2.3), we focus on the model's ability to capture the mechanistic interactions, instead of matching the observations for the wrong reasons. In fact, we expect that the model will partition the extra rainfall (the wet bias) into both increased ET and increased river discharge, the balance between the two depending on the dominant control of ET. For example, if the extra rain occurs in the wet season, it should increase river discharge more than ET because ET is not water limited, but if the extra rain occurs in the dry season, as is the case here with the Interim rainfall forcing (*Miguez-Macho and Fan* [2012, Figures 6 and 7] and Figure 5), then it should increase ET more than river discharge because ET is more water-limited and sensitive to the added moisture.

3.1. Comparison With Observed Soil Moisture

[32] We found soil moisture observations in seven published reports as given in Table 1 with the locations roughly shown in Figure 6. A quick comparison between the model soil (Figure 4a) and the observation site soil (Table 1, second to last column) reveals large discrepancies between the two. While sandy soil is reported at all sites except for Asu (plateau), Tapajos, and Juruena (uplands), the corresponding model soil is exclusively clay loam (class 8) and clay (class 11). Sandy soils and clay soils differ hydraulically in several ways. First, clay soils have higher porosity and wilting point water content, leading to generally higher volumetric water contents (a shift). Second, clay soils don't receive and drain efficiently as in sand in the wet season. Third, clay soils can pump stronger upward capillary fluxes in the dry season. These differences cause the model, with mostly clay soils over the Amazon, to produce much reduced depth and temporal variations in soil moisture. Depth-wise, sandy soils typically exhibit a large vertical gradient with dry soil on the top and wet soil near the water table, while clay soils tend to have a more uniform profile. Temporally, sandy soils fill and drain quickly, while clay soils will respond to longer time scale forcing changes. Therefore direct model-observation comparison in the absolute values of volumetric soil water content can be problematic.

[33] The problem stems from the lack of the observed fine-scale soil heterogeneity in global soil data sets. This underscores a fundamental data deficiency hampering the use of detailed process-based models and a need for a community-level effort to produce such a data set. Lacking alternatives at the present, we compare the modeled and observed effective soil saturation, defined as (volumetric soil moisture – residual water content) / (soil porosity – residual water content), giving the fraction of maximum soil water available for ET use. This scaling removes the effect of difference in porosity and residual water content, but not the difference in drainage and capillary rise. Soil porosity and residual water content for the observations are given in some of the published reports, while others discussed periods and depths of saturation, and the associated maximum water content was used as porosity. When the only information given is a general description (second to last column, Table 1), we classify the site into one of the 12 standard soil texture classes (Figure 4a) but constrain the standard parameters with the observed maximum and minimum water content; i.e., if the standard porosity is less than the observed maximum, or the standard residual water content is greater than the observed minimum, the latter are used instead. The values used are given in the last column of Table 1.

[34] Figure 6 plots the observed (symbols) and modeled (lines) effective saturation at these sites at the observation time steps (daily, weekly, or monthly) over the overlapping period. We point out the major model-observation differences. First, the model lacks moisture variation with depth at Asu (slope base, sandy soil reported at site) and Jaru

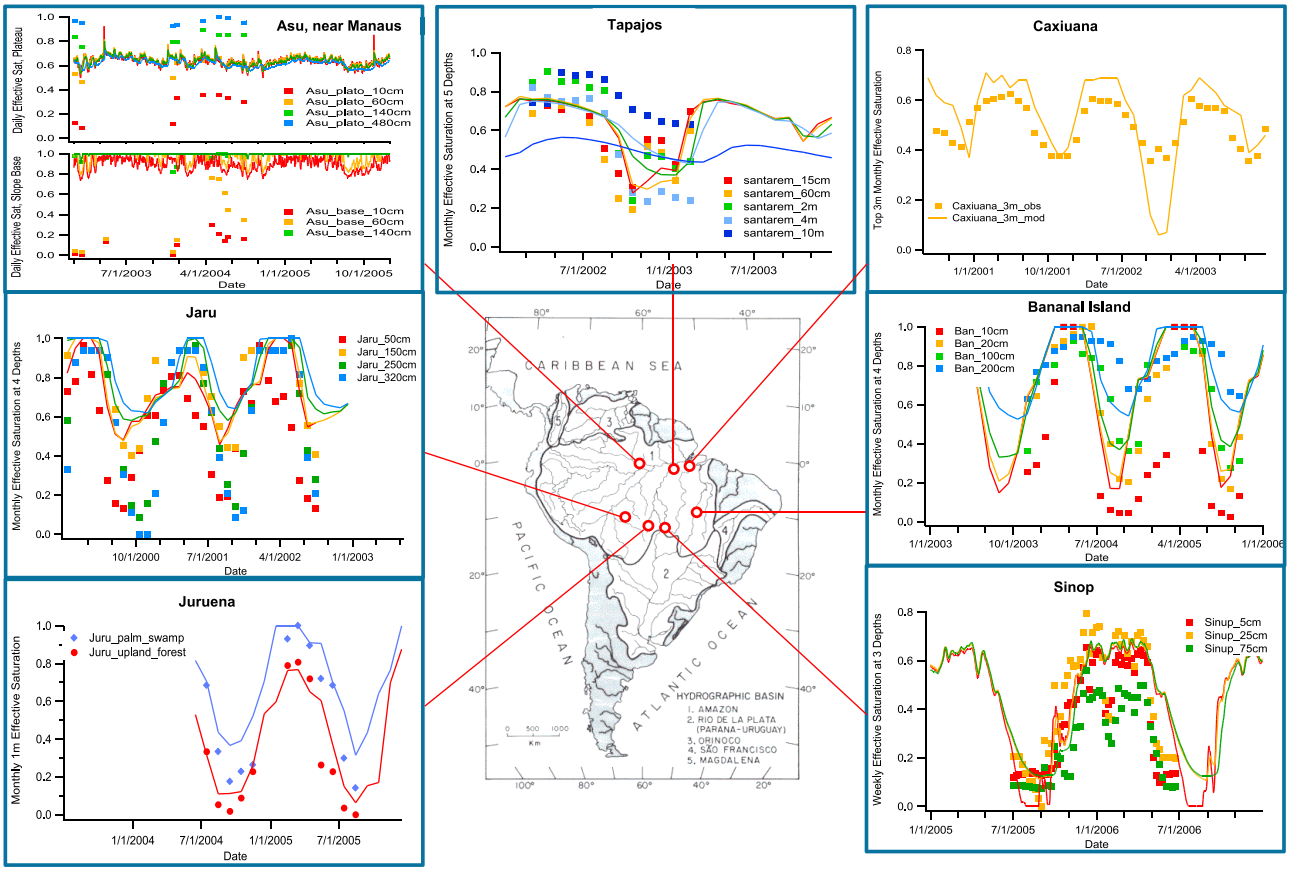

Figure 6. Comparison with observed soil moisture at 7 sites with published data, shown as effective saturation, or the ET available soil water.

(medium-textured soil over saprolite at site) due to poor drainage and high capillary rise in clay soils in the model. The shallow water table here exacerbates the capillary rise. Second, this lack of depth variation is also apparent at Asu-plateau and Tapajos where the soil types agree (clay oxisol) between model and sites, but the issue is the unique tropical soils as noted by *Tomasella et al.* [2000] that drain like sand but hold on to moisture like clay due to the formation of clay aggregates, while the widely used pedo-transfer functions are based on temperate soils of North America and Europe. The efficient drainage in the tropical clay soils leads to drier shallow soils. Third, the small seasonal amplitude in the Interim rainfall forcing, particularly in the northwestern Amazon (*Miguez-Macho and Fan* [2012, Figure 7] and Figure 5) further compounds the poor drainage in the model soil, leading to smaller seasonal changes than observed at Asu, Jaru, and Tapajos. But in general, the magnitude and seasonal patterns between the observations and model results are consistent.

3.2. Comparison With Observed ET Fluxes

[35] We compare the simulated seasonal patterns of ET flux with the observations given by *da Rocha et al.* [2009] at six LBA sites in the Amazon, shown in Figure 7. For reference, the upper panels give the monthly rainfall from the merged gauge-satellite observations of GPCP (blue) and the ERA-Interim forcing (red). In the lower panels, the model ET (red) is broken down to three components: interception (gray), transpiration (green), and surface evaporation (brown). At the three northern sites, dry season ET is substantially higher in the models, a direct consequence of the large high bias in dry seasonal rainfall forcing, which is carried over to the following wet season. At the three southern sites, the smaller rainfall forcing bias leads to a smaller model departure. We note that the wet-bias in the Interim rainfall forcing not only lead to higher ET fluxes but also higher river discharge [*Miguez-Macho and Fan*, 2012, Figure 7], as expected without model calibration to match one of the water budget partition terms alone.

[36] At all sites, the seasonal amplitude in the models is greater than in the observations despite the smaller rainfall seasonality in the forcing, likely linked to the lack of atmospheric feedback to ET in off-line simulations such as this; since the atmospheric forcing is prescribed, the high ET rate due to high rainfall, e.g., does not raise surface humidity accordingly which serves to reduce atmospheric vapor deficit and limit ET in nature and in coupled simulations.

[37] Other factors, such as model-site departure in soil hydraulic properties as discussed earlier, in vegetation biophysical parameters such as LAI, albedo, roughness heights and rooting depths, also play important roles. Without close agreements between model and site characteristics, accurate atmospheric forcing and land-atmosphere feedbacks, and without parameter tuning, it is expected that the model and site observations will not fully agree with one another.

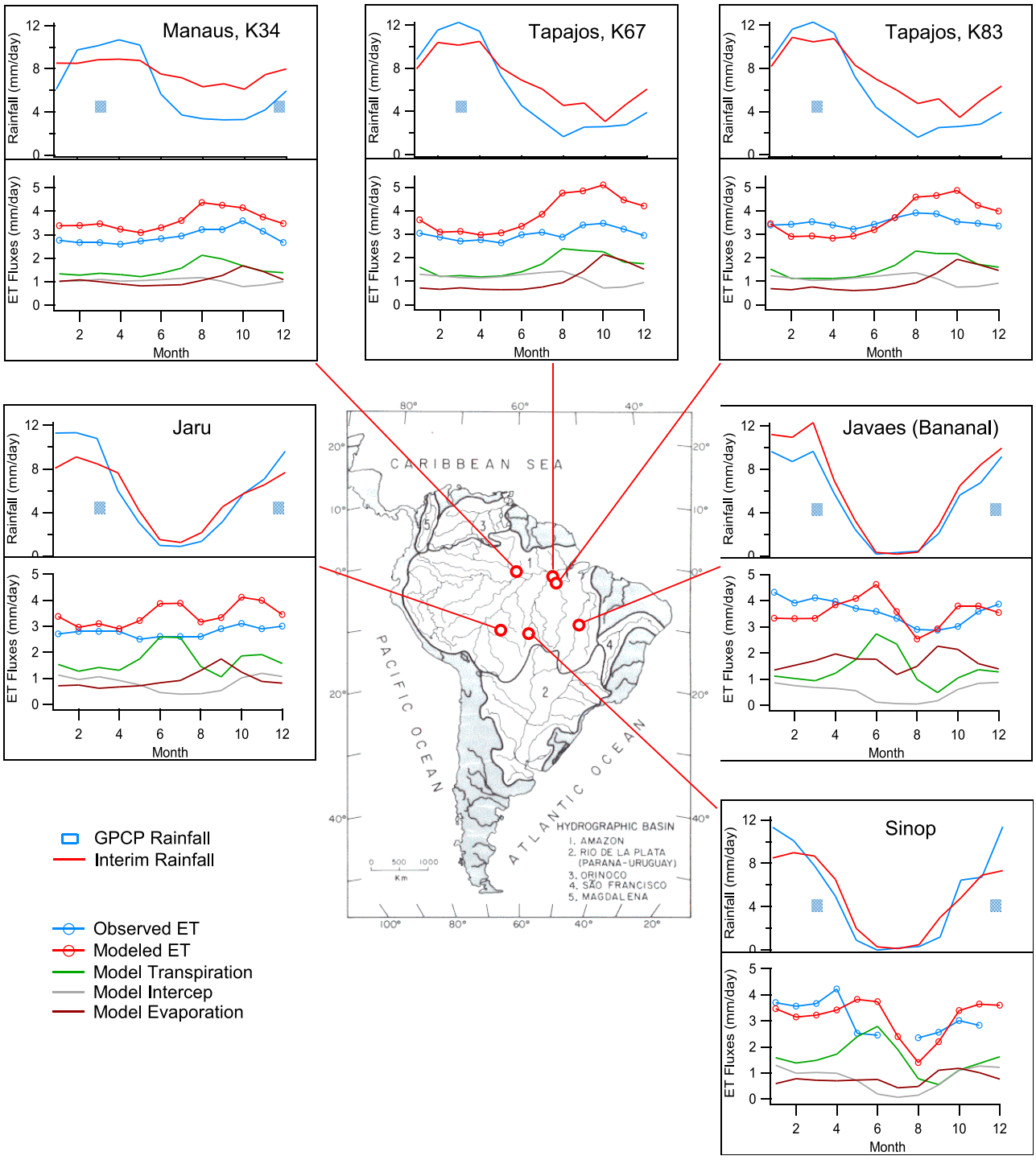

Figure 7. Comparison between simulated and observed seasonal patterns of ET (lower panel) from *da Rocha et al.* [2009], with GPCP and Interim rainfall shown (top panel).

[38] We also compare the model interception loss with observations at two sites reported in the literature. Near Manaus, *Cuartas* [2008], based on 5-min stemflow and throughfall measurements over 2002–2004, report 13.3% in a normal year and 22.6% in a drier year, and 13.9–21.4% in the wet season and 12.0–25.0% in the dry season. The model mean over 2000–2006 gives 13.5% annually, 12.0% in the wet season and 15.5% in the dry season, agreeing well with the observations. Near Santarem, *Czikowsky and Fitzjarrald* [2009], based on a new method using eddy-covariance flux measurements over 2001–2003, report 10% for moderate rain-rate daytime events, 18% for light events, and 7.8% for heavy events, with the mean for all daytime and nocturnal events of 11.6%. The model mean over 2000–2006 gives 16.7% annually, 13.8% in the wet season, and 20.6% in the dry season, which are much higher than from the new method. Since the dry season is longer at Santarem than at Manaus, it is possible that interception is higher at Santarem,

which is what the model suggests, contrary to the two isolated observations using different methods. We also note that where extensive flooding occurs, such as at Javaes (Bananal Island), surface evaporation (either from bare soil or floodplain surface) can exceed transpiration and become the dominant term in the total ET flux in the flooding season, as discussed in *Borma et al.* [2009].

[39] In general, the model produces a seasonal dynamics in soil moisture and ET fluxes that are comparable to the available observations. The model has a wet bias particularly in the dry season due to biased forcing, biased soil properties, and the lack of land-atmosphere feedbacks. We note that without model tuning, these biases and the missing land-atmosphere feedback in off-line simulations cannot be absorbed into the tuned parameters and hence are faithfully reflected in the simulation results. A key question here is how the model bias affects our investigation into groundwater's role in regulating seasonal dynamics of soil moisture and ET. On one hand, the biased-high dry season rainfall directly supplies model ET, reducing surface drought and hence the need for the deeper source. On the other hand, the prevalence of clay soils in the model exaggerates the capillary rise from the water table. How these two effects counteract is unclear. To tease out the influence of the groundwater given these model uncertainties, we will conduct a parallel model run without the groundwater but with free drainage at the bottom of the model soil column, a standard approach in large-scale land models. Both model experiments will be subject to the same forcing and soil biases as well as the lack of atmospheric feedbacks, and their difference should better reflect the role of the groundwater. In the following discussions where local water balance is the focus, we will also choose sites in the Amazon that avoid the rainfall and soil bias, such as the southeastern Amazon as shown in the gray box in Figure 4a, which includes sandy-loam (class 3) and sandy-clay-loam (6) and has more realistic dry season rainfall forcing (Figure 5, between Jaru and Bananal Island), yet the model land cover remains tropical forest.

4. Results: Groundwater Influence on Amazon Seasonal Soil Moisture and ET

[40] We test the importance of the four mechanisms proposed earlier whereby groundwater can regulate the seasonal dynamics of soil moisture and ET flux in the Amazon. To reduce the spin-up effect, we discard the first year where mean seasonal dynamics is the focus.

4.1. Mechanism-1: Shallow Groundwater Can Directly Support Plant Uptake

[41] We proposed that the water table can be sufficiently shallow to be directly accessible to plant roots under portions of the Amazon at least seasonally. This is schematically illustrated in Figure 1a. Syntheses of global observations [*Schenk and Jackson*, 2002] suggest that the bulk of root mass is found in the top 2 m soil, but the maximum rooting depth can be tens of meters in arid regions [*Canadell et al.*, 1996]. In the Amazon, roots were found at 18 m deep under the forest in Tapajos [*Nepstad et al.*, 1994]. Given the wide range of reported rooting depths depending on climate, soil and vegetation, we examine the model simulated spatial and temporal frequency of shallow groundwater occurrence. The question is, what is the likely area fraction of the Amazon with a water table within the rooting depths, and how does that fraction change through the seasons?

[42] Figure 8 shows the simulated monthly (Jan, Apr, Jul, and Oct) water table depth (WTD) over the Amazon (top panels) with local details in the Tapajos drainage (middle), and the area fraction of WTD intervals over the whole basin (bottom). As shown in the histograms, a substantial area of the Amazon can experience water table conditions less than 2 m deep, which is within the standard plant rooting depth commonly assumed for forest vegetation in large-scale land models. This fraction is 40% in January (peak wet season), 48% in April (late wet season), 36% in July (peak dry season), and 25% in October (end of dry season) based on our simulations. Although the numbers themselves may include forcing and parameter biases discussed earlier, it is likely that this fraction is not a negligible number. Modeled shallow water table is mostly found under the large floodplains (top panels, purple) and along the river valleys (middle panels, purple and blue). Even at the peak and late dry season (Jul–Oct), more than 20% of the Amazon can have its water table in the root zone, which is mostly located in the low and flat foreland basins and central floodplains, in agreement with the existence of extensive swamp forests found in these places.

[43] Under topographic highs, modeled WTD ranges from 5 to 40 m across most of the Amazon and across the seasons. At the transition between valleys and plateaus, it varies between 3 m to 5 m, which, given the range of reported rooting depths of Amazon forest species, may be accessible to some roots. The area fraction of 3–5 m WTD is 19% in January (peak wet season), 16% in April (late wet season), 26% in July (peak dry season), and 30% in October (end of dry season) based on the simulations. These fractions suggest that the lower terra-firme species may also directly access the water table, particularly in late dry season when it is the shallowest under high grounds. The seasonal timing of different WTD zones is further discussed in section 4.4.

4.2. Mechanism-2: Shallow Groundwater Can Impede Drainage in the Wet Season

[44] We proposed that where the water table is shallow, drainage in the wet season can be significantly reduced, leaving a larger soil water store at the beginning of the dry season and giving the Amazon forest a stronger start. This is schematically illustrated in Figure 1b, where a fixed-depth soil column with free drainage (red box) correctly describes the drainage mechanism under the high grounds where the water table is below the model column, but it artificially accelerates drainage near the valleys where the water table is within the model column. We test this hypothesis by contrasting the results from two parallel model simulations, one with the fully coupled groundwater-soil water store, and the other with a fixed soil column of 4 m depth (deeper than commonly assumed) with free drainage at the bottom driven by gravity and controlled by the hydraulic conductivity at the water content found at the bottom layer. We refer to the former as the GW experiment and the latter as the FD experiment. Both simulations have identical setup including the initial soil moisture as determined from the initial water table.

[45] Figure 9 plots the modeled annual mean soil drainage flux averaged over the later 10 yrs (2001–2010) of the

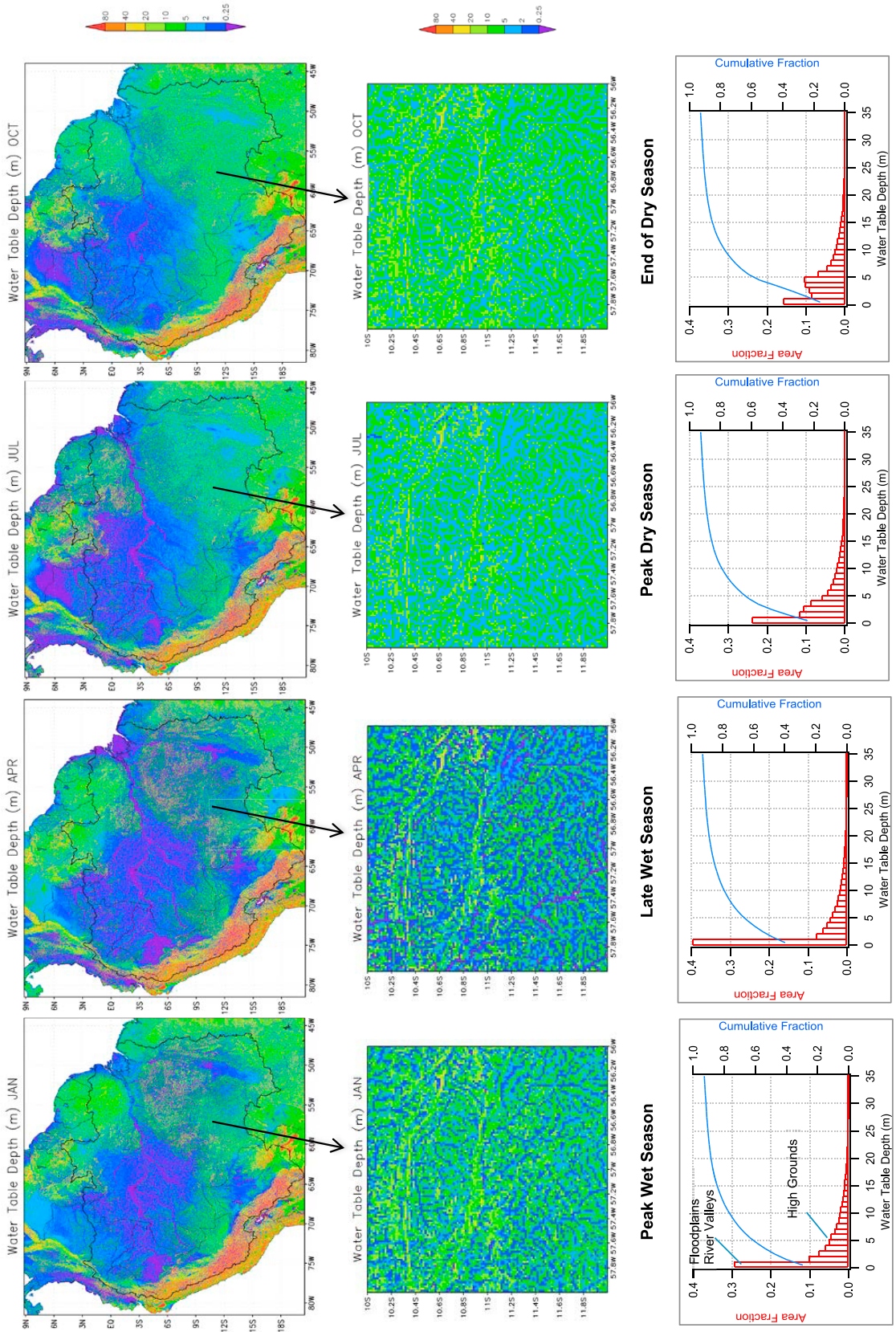

Figure 8. (top row) Seasonal water table depth in the Amazon. (middle row) Local details in headwater Tapajos-Xingu. (bottom row) Water table depth distribution over the Amazon (red: area fraction, blue: cumulative area fraction).

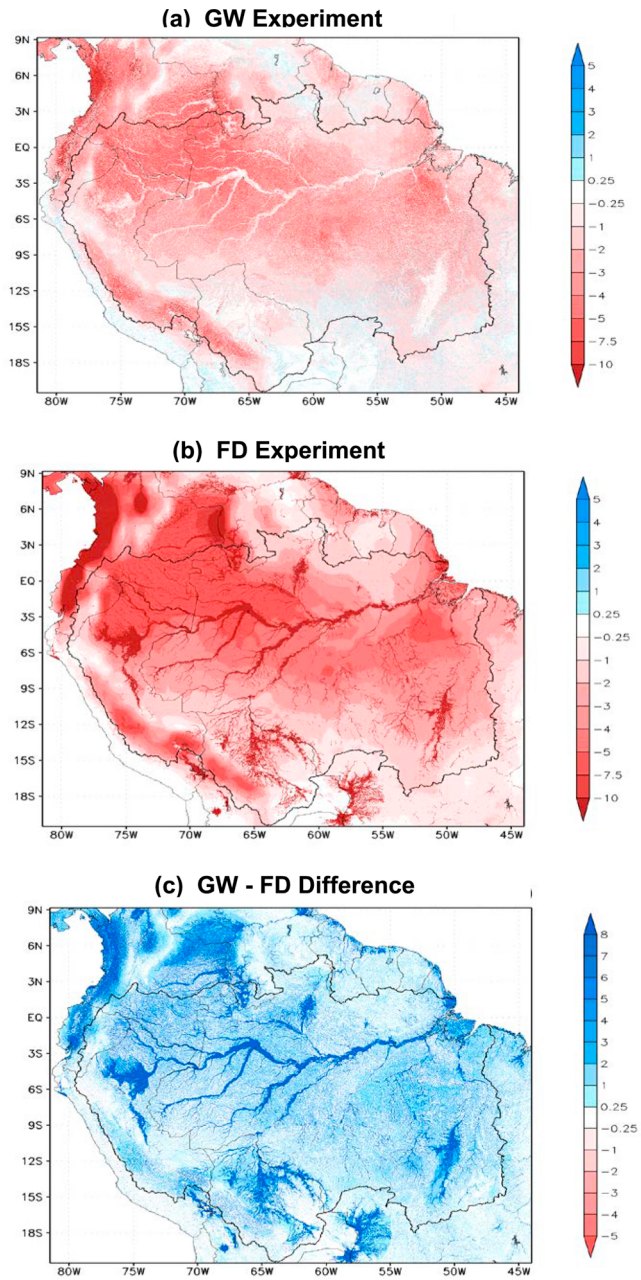

Figure 9. Annual mean soil drainage flux (mm/day) from (a) the coupled groundwater and (b) free drainage where negative is downward flux, and (c) the difference.

simulation (discarding year 1). This flux, in the GW experiment, is the exchange between the unsaturated soil zone and the groundwater below, i.e., the flux across the water table, which is recharge in response to rainfall and discharge in response to surface ET and hence can go both ways. In the northern and southern edges of the Amazon where seasonality is strong, the simulated annual net flux can be upward, sustaining ET, and this net groundwater loss to the soil and the atmosphere is in turn sustained by lateral convergence of groundwater from higher neighboring grounds. In the FD experiment, this flux is the water leaving the fixed-depth 4 m soil column and removed from soil storage, and it is pointed downward always. It is clear that the simulated soil drainage loss is substantially higher in FD, most pronounced in the floodplains and river valleys where the water table is shallow (Figure 9c, dark blue); the modeled water table control on floodplain infiltration loss has been analyzed in detail in the companion paper [see *Miguez-Macho and Fan*, 2012, Figure 13 and section 5.2]. Note that the large infiltration loss from FD is placed in the river network and routed out of the model cells, no longer available for later ET use. Little difference is found on high grounds (white in Figure 9c) where FD adequately describes soil drainage physics.

[46] Figure 10 gives the seasonal breakdown of Figure 9. The large blue patches in the GW experiment (top panels) migrate from the northern hemisphere in January (northern dry season) to the southern hemisphere in July (southern dry season) when the flux is upward driven by capillary force, sending groundwater to the soil stores in response to surface ET demands. In the FD experiment (middle panels), the same regions show zero flux in the dry season because there is no more water to drain and no deeper source to tap. During the wet season, soil drainage loss is significantly greater in the FD experiment (darker red). In the GW experiment, deep drainage continues in the dry season if the soil water content is still above field capacity in the deeper layers, as observed in nature [e.g., *Juárez et al.*, 2007], which is why the GW experiment has more drainage loss than FD in the dry season (Figure 10, difference map, bottom panels, red color).

[47] The much reduced drainage in the wet season in the GW run means a larger soil water store at the beginning of the dry season, giving the modeled Amazon soil a fuller store at the beginning of the dry season. This is shown in Figure 11, where the top 2 m soil moisture is substantially different between GW and FD not only in the dry season, but also in the wet season. The higher soil store at the beginning, plus the upward capillary flux from the water table later in the dry season, discussed next, can help maintain a wetter root-zone soil throughout the year.

4.3. Mechanism-3: Shallow Groundwater Can Sustain Capillary Rise

[48] We proposed that where the water table is below the rooting depth but within the reach of capillary rise, the latter can send water upward into the root zone, as schematically illustrated in Figure 1c. This function can be important in the dry season when the top is dry, creating an upward matric-potential gradient, particularly in clay soils where the large particle surface-area and the narrow pores create a strong suction force with possible capillary rise of tens of meters [*Freeze and Cherry*, 1979].

[49] The simulated capillary flux is reflected in Figure 10 where the flux across the water table is seasonally reversed (top panels, GW run); During the dry season, Jan–Apr in the northern and Jul–Oct in the southern hemisphere, the flux is upward (blue). This capillary withdrawal from the groundwater only resided briefly in the soil zone due to the high surface demand this time of the year and is not strongly reflected in the soil moisture maps of Figure 11, before it entered the ET stream, as shown in Figure 12. The simulated ET difference between GW and FD (Figure 12, bottom row) is substantial in the respective hemispheric dry seasons. Note that the FD experiment gives higher ET on the floodplains because it produces more floodwater in the wet season with uninhibited soil drainage and large influx into the river-

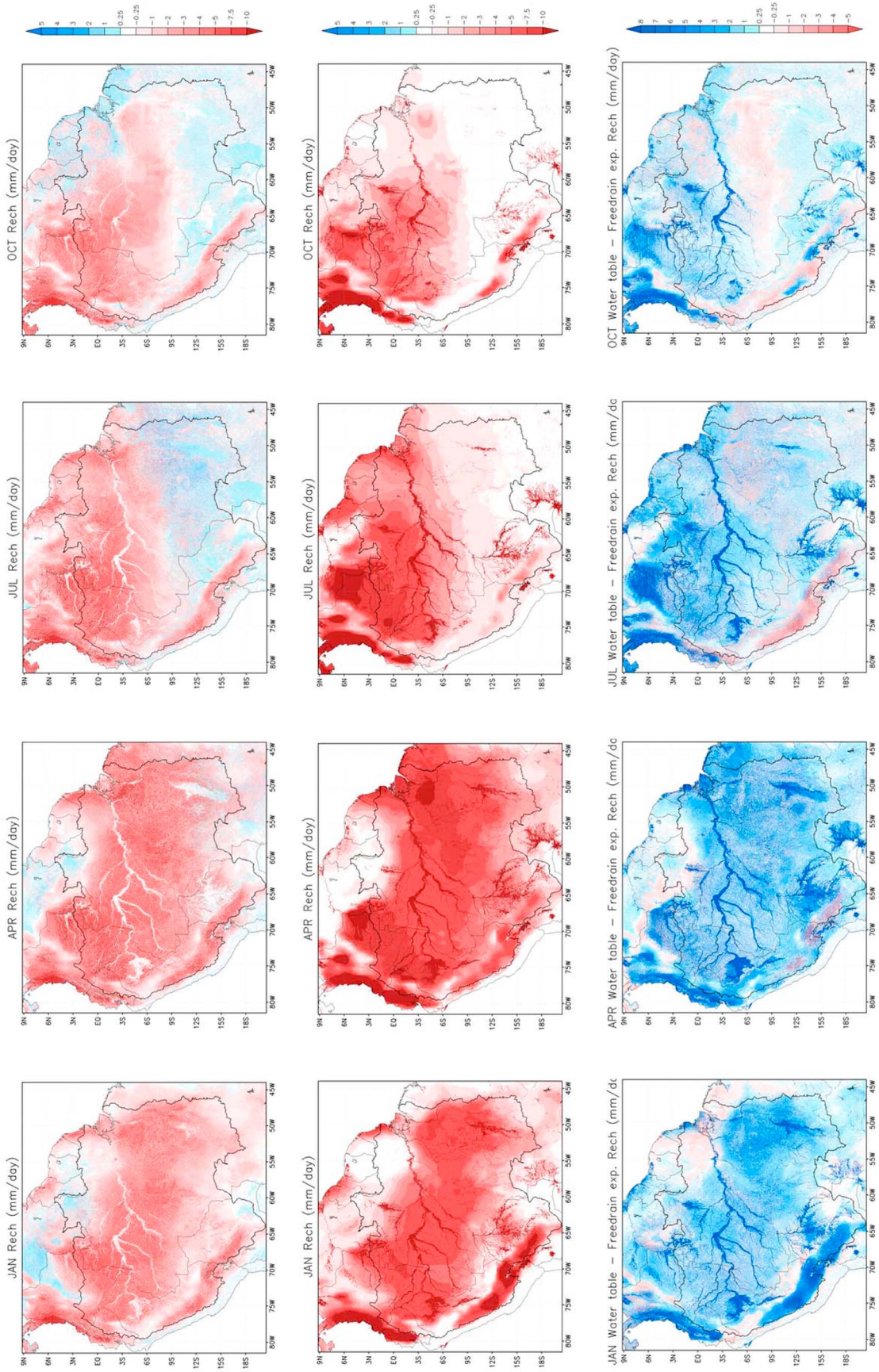

Figure 10. Seasonal soil drainage flux (mm/day) from (top row) the coupled groundwater (GW), (middle row) free drainage (FD) model experiments, and (bottom row) their differences.

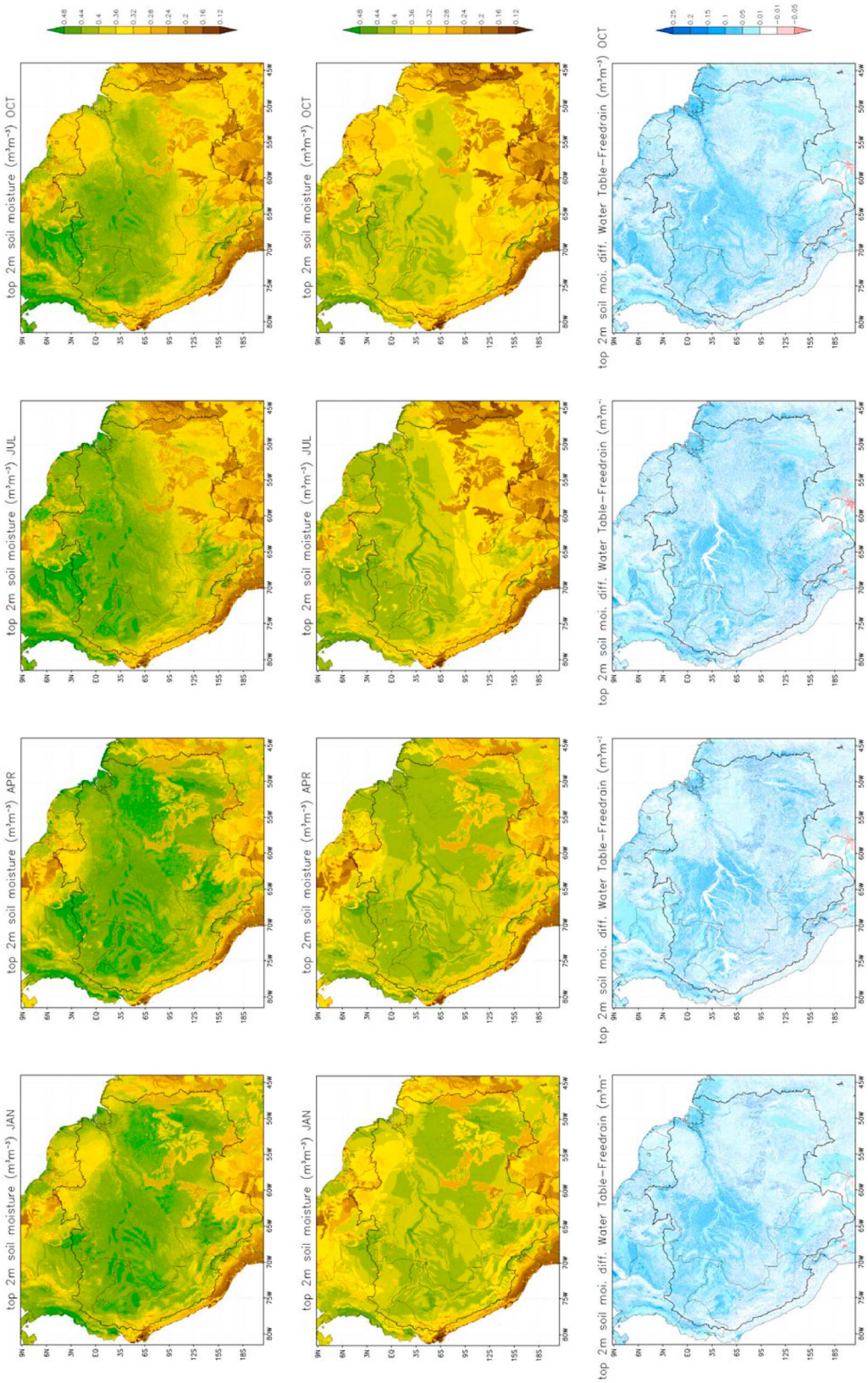

Figure 11. Seasonal top 2 m volumetric soil moisture from (top row) the coupled groundwater (GW), (middle row) free drainage (FD) model experiments, and (bottom row) their differences.

floodplain system from the uplands. The memory of it in the 4 m soil column gives slightly higher ET here.

[50] Figure 13 offers a closer look at the simulated seasonal changes in the soil water and groundwater stores at a terra-firme site and a valley site. The sites are within the box in Figures 4a and 12. They are located in the Tapajos drainage with strong seasonal rainfall, but the least dry season rainfall forcing bias (Figures 5 and 7 and *Miguez-Macho and Fan* [2012, Figures 6 and 7]) and include sandy soils (Figure 4a, class 3 and 6), to reduce the associated model uncertainties. The model vegetation is broad-leaf forest with rooting depth to 1.5 m. As schematically illustrated to the left of Figure 13, the simulated soil water and groundwater stores are coupled through the fluxes between, i.e., drainage (D) and capillary rise (C), where L stands for lateral groundwater flow to adjacent cells. The model water table varied between 13 and 21 m below the terra-firme site and 0–6 m below the valley site. Results from FD are also plotted as (+) symbols wherever relevant. We highlight the following.

[51] At the terra-firme site, the simulated water table is far below the 4 m soil column, and FD gives nearly identical soil moisture storage and ET fluxes as GW. The only difference is that FD has a greater drainage loss in the wet season and no loss in the dry season, while in GW soil drainage continues into the dry season. But what occurs at these greater depths does not influence the near surface soil moisture and ET fluxes. Therefore, where the water table is deep and the soil has good drainage, the water table matters little to seasonal ET. However, it does affect the streamflow in its groundwater contribution; the steady drainage of soil water (D) into the groundwater system, and the latter's steady convergence (L) into the valley before it enters the stream, dampens the seasonal amplitude in valley soil moisture, stream discharge and its geochemical characteristics. No surface runoff is produced in both GW and FD runs at this high point (hence not shown).

[52] At the valley site, the water table in the GW run fluctuated in and out of the 4 m soil column, affecting all fluxes by the following means. First, it changed the partition at the land surface between infiltration (I) and surface runoff (S). In the GW run, infiltration is often inhibited by the shallow water table (middle panel); meanwhile the rising water table creates surface saturation and saturation-excess surface runoff (or Dunne runoff, shown in red). The timing of this runoff lags behind infiltration as the latter slowly raises the water table, causing it to happen. In the FD experiment, infiltration is uninhibited and surface runoff only occurs when rainfall exceeds infiltration rate (infiltration-excess runoff, or Horton runoff). During the same period when surface runoff is strong in the GW run, infiltration is strong in the FD run. Thus the presence of the shallow water table alters the runoff pathways. Second, the shallow water table alters what happens at the base of the unsaturated soil, i.e., the drainage of soil water (D) and the upward capillary flux (C). In the GW experiment, wet season soil drainage is far smaller, and dry season capillary flux is significant. At daily time steps (not shown), capillary flux often exceeds drainage input, the difference afforded by groundwater convergence from uplands. This lateral convergence, shown in red in the bottom panel, feeds groundwater discharge into the streams (base flow) as well as valley ET fluxes. For the soil water store, the smaller drainage and the strong upward capillary flux cause it to be larger in the GW run in both wet season (small drainage) and dry season (large upward capillary flux), and hence larger ET flux in both seasons. We note that the overly abundant clay soils in the model, despite our selecting a region with the most sandy soils for this analysis, may have exaggerated the strength of the capillary force, and hence the results discussed here should be interpreted only qualitatively.

4.4. Mechanism-4: Groundwater Can Provide the Dry Season Buffer for Soil Moisture and ET

[53] We proposed that, due to its delayed and dampened response to seasonal rainfall, the timing of groundwater can be one of the reasons behind its buffering effect for dry season surface stress. Across the Amazon, it has been shown that the water table reaches its seasonal peak weeks to months after the peak seasonal rainfall, and the surplus/deficit in groundwater stores from one season can carry over to the next, as referenced earlier. This is schematically illustrated in Figure 1d; below the hilltop, the modeled water table is deeper with longer-delayed response to seasonal rainfall; near the valley, the modeled water table is shallower with shorter-delayed response. The months of delay cause the modeled groundwater to be the shallowest when the surface is dry, maximizing vertical moisture gradient and its influence on the surface as a source from below.

[54] To test the idea of a sequential delay in water table response from high grounds to valleys, we plot in Figure 14 the simulated mean seasonal cycle of water table depth and the lateral groundwater convergence from hills to valleys at the same terra-firme and valley sites shown in Figure 13. Seasonal rainfall peaks in February, with the simulated water table peaking at 1–2 months later at the valley site (green), and 3–4 months later at the terra-firme site (green-dash), consistent with the observations reported in the literature referenced earlier. Based on Darcy's law, the lateral groundwater convergence from the terra-firme to the valley is determined by the head difference between the sites (dh) multiplied by the flow cross section height (h, analogous to the width of a flow pipe), the latter can be approximated by the mean water table head at the two sites. This quantity (dh $\times$ h), scaled to 0–1 to fit in the graph, is shown in blue. Its timing coincides with the lateral gain of groundwater (solid red) at the valley site as expected. Note that the modeled groundwater convergence terms have very weak seasonal amplitudes compared to rainfall. At the valley site, the simulated groundwater input is greater than rainfall input in the dry season (solid red line crossing rainfall), keeping the valleys wet when rain fails to come. This temporal buffer is provided by the slow groundwater convergence in the model.

[55] This temporal buffer may also manifest itself as spatial patterns. It can be seen in the water table depth distribution (Figure 15, top row) in mid Tapajos drainage (box in Figures 4a and 12) for the month of February and August. The topographic structure, which drives groundwater convergence, persists throughout the seasonal cycle. This persistent structure is in turn reflected in the root zone soil water distribution (middle row), but the influence of soil properties begins to emerge. Yet within each soil class, the hills and valleys are clearly differentiated. The ET flux involves additional drivers, particularly available energy; in the peak

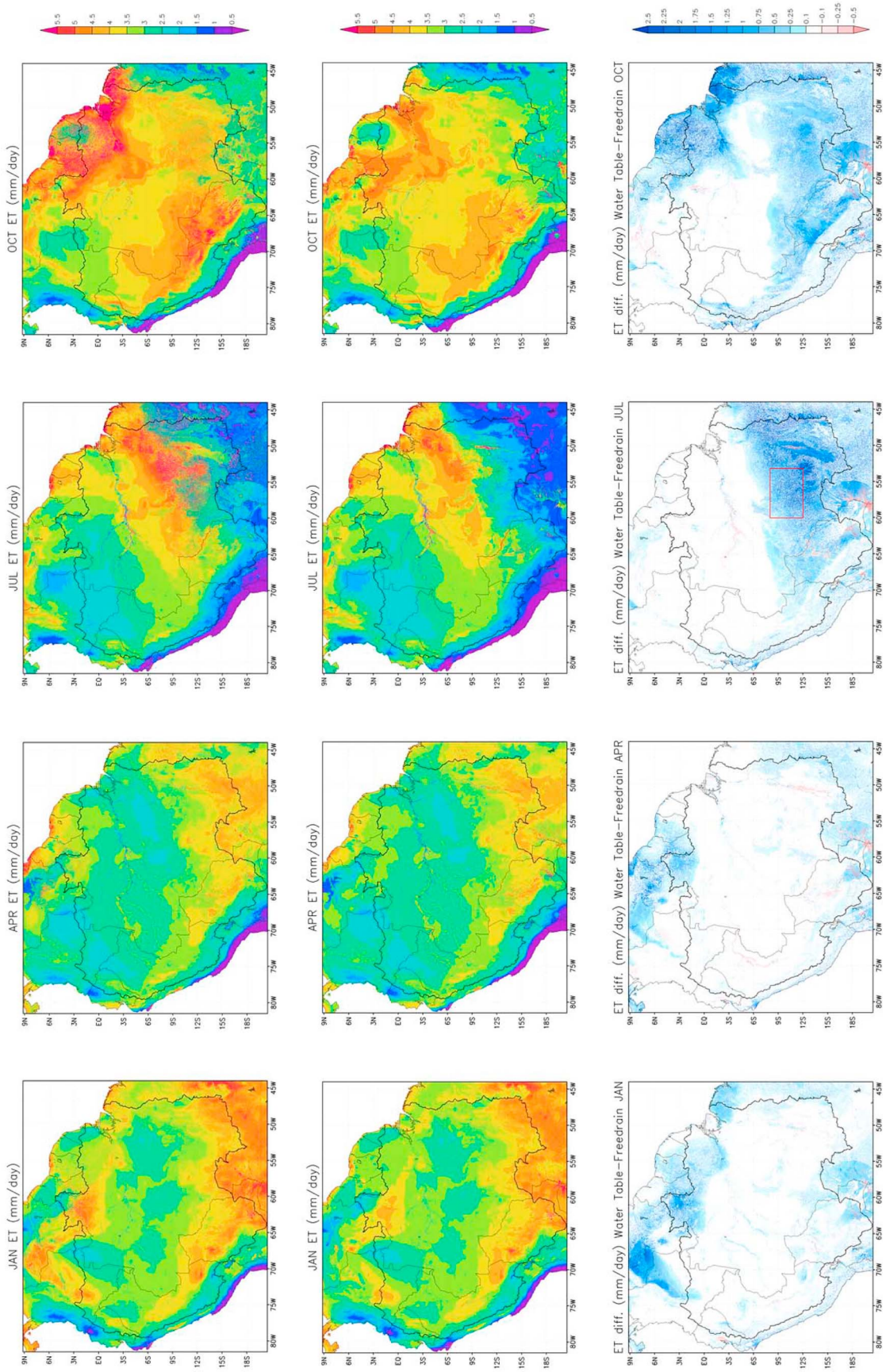

Figure 12. Seasonal ET flux from (top) the coupled groundwater (GW), (middle row) free drainage (FD) model experiments, and (bottom row) their differences. The red box is the area for local studies later.

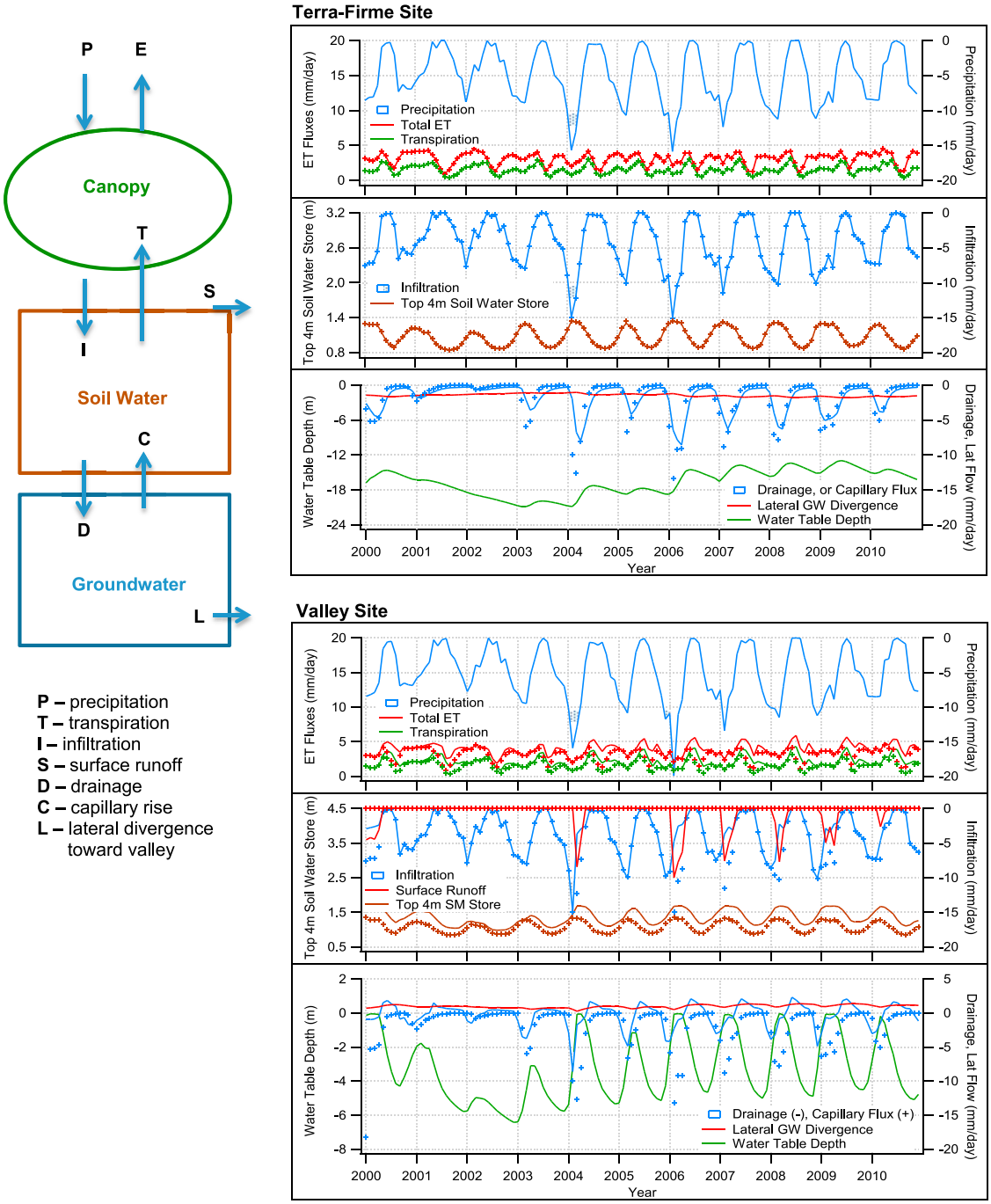

Figure 13. Monthly coupled evolution of soil and groundwater stores via exchange fluxes, and their influence on ET at 2 model cells in the Tapajos basin. Results from the GW run are shown as lines and FD as symbols where relevant.

wet season soil water is not limiting and hence the topographic structure is largely absent, but in the peak dry season when soil water is indeed limiting, the topographic structure again emerges, creating sharp contrasts between hill and valley ET rates. It is known that the shallow groundwater in the valleys supports lush gallery forests along river corridors in the otherwise dry Cerrado landscape further east [*Prance*, 1987; *Clapperton*, 1993]. This result suggests that at least a fraction of the dry season Amazon forest continues to transpire in the model. If this is indeed the case in nature, lateral groundwater convergence, with its slow and stable characteristics, is a key process that enables this to happen.

5. Summary and Discussions

[56] Discrepancies between observations and models regarding the Amazon seasonal soil water stress have stimulated much discussion in recent years, and several mechanisms have been proposed to explain the lack of observed soil water stress in the dry season. Motivated by

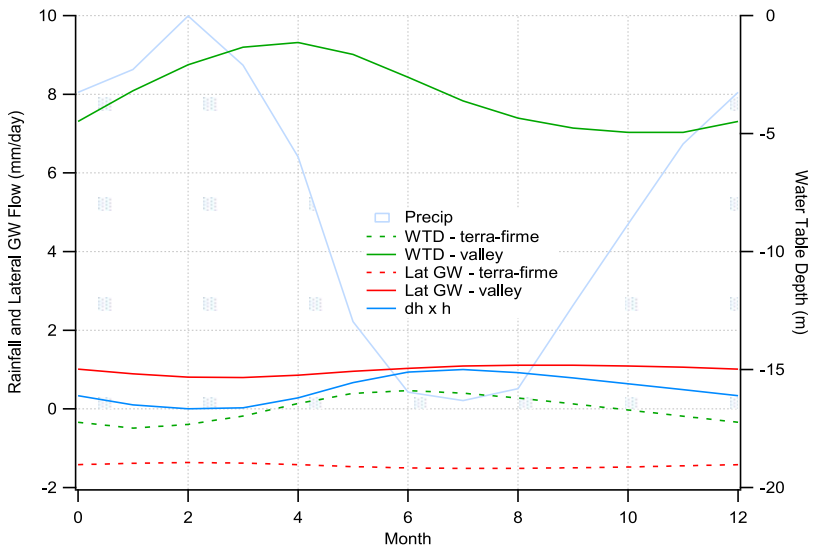

Figure 14. Mean seasonal cycle of water table depth and lateral groundwater convergence at the terra-firme and valley sites (where dh × h is the product of hydraulic head difference and lateral flow cross-section height, indicating the potential for lateral groundwater flow). Seasonal rainfall is plotted for reference.

field observations of shallow water table presence (e.g., *Brazilian Geological Survey* as compiled in *Fan and Miguez-Macho* [2010]; *Bongers et al.* [1985]; *Poels* [1987]; *Lesack* [1995]; *Coomes and Grubb* [1996]; *Hodnett et al.* [1997a, 1997b]; *McClain et al.* [1997]; *Selhorst et al.* [2003]; *Grogan and Galvão* [2006]; *Jirka et al.* [2007]; *Tomasella et al.* [2008]; *Cuartas* [2008]; *Vourlitis et al.* [2008]; *Borma et al.* [2009]; *Lähteenoja and Page* [2011]; and *Neu et al.* [2011]), we evaluate the role of the groundwater in buffering the dry season soil moisture stress and ET. We use a fully coupled groundwater-surface water model called LEAF-Hydro-Flood, forced with ERA-Interim reanalysis, at 2 km grid resolution, 4 min time steps, and over the 11 year period of 2000–2010. The simulation is validated with observed daily stream discharge, water table depth, and seasonal flooding in the companion paper, and further tested here with the available observations in soil moisture and ET fluxes. To reduce model uncertainty on our conclusions, a parallel simulation without the groundwater is conducted to bring out the influence of the groundwater in the presence of biases in dry season rainfall forcing and soil hydraulic properties from standard global soil data sets. Based on the simulation results, we tested the relevance of four mechanisms whereby the groundwater can influence the land surface. First, a shallow water table can be a direct source for plant uptake. This is supported by the results shown in Figure 8; the simulated water table in the range of 0–2 m deep occupies 20–40% of the area in the Amazon across the season. This depth is within the rooting zone of forest vegetation in standard land model parameterizations. Second, where the water table is shallow, drainage in the wet season can be significantly reduced, leading to a larger soil water store at the beginning of the dry season. This is supported by the results shown in Figures 9 and 10, where uninhibited drainage in the FD experiment regardless of water table depth leads to a much drier soil in the wet season, as shown in Figure 11. Third, where the water table is not far below the rooting depth, capillary rise from the water table can reach the rooting zone and sustain dry season ET. This is supported by the results shown in Figure 10 where the modeled dry season exchange between the soil water and the groundwater is upward, directly supplying model ET as shown in Figures 12 and 13 at the valley site. Fourth and lastly, the delayed and dampened response of groundwater to seasonal rainfall can be one of the mechanisms whereby groundwater buffers dry season surface stress. This is supported by the results shown in Figure 14 where the valley water table reaches its peak 1–2 months after peak seasonal rain in the valleys, and 3–4 months after under the uplands, causing the model groundwater to be the shallowest when the surface begins to dry. This temporal delay can also express itself as a spatial pattern as shown in Figure 15; throughout the dry season, continued groundwater convergence in the model maintains moist valleys all year-round and forms a structured mosaic of wet-dry patches in the dry season, sustaining high model ET at least in the lower parts of the Amazon landscape.

[57] Returning to the observation-model discrepancy regarding the Amazon dry season ET, we now examine the modeled ET difference between the GW and the FD experiments. As shown in Figures 11 and 12, regions of largest soil moisture difference do not map into regions of the largest ET difference because the dependence of ET on soil moisture is not linear. If the soil moisture content is already sufficient to satisfy the atmospheric demand of ET, an increase of the water content in the soil will not translate into an increase in ET. Atmospheric demand is only stressful in the respective hemispheric dry season, when the lack of rainfall combined to high ET rates can deplete the soil moisture store to the point when it becomes the limiting factor for ET. It is reasonable to say that the presence of the groundwater in the model made little or no difference to ET in the central Amazon where the seasonality is small. This is partly because that the 4 m soil column in the FD run has a sufficient soil

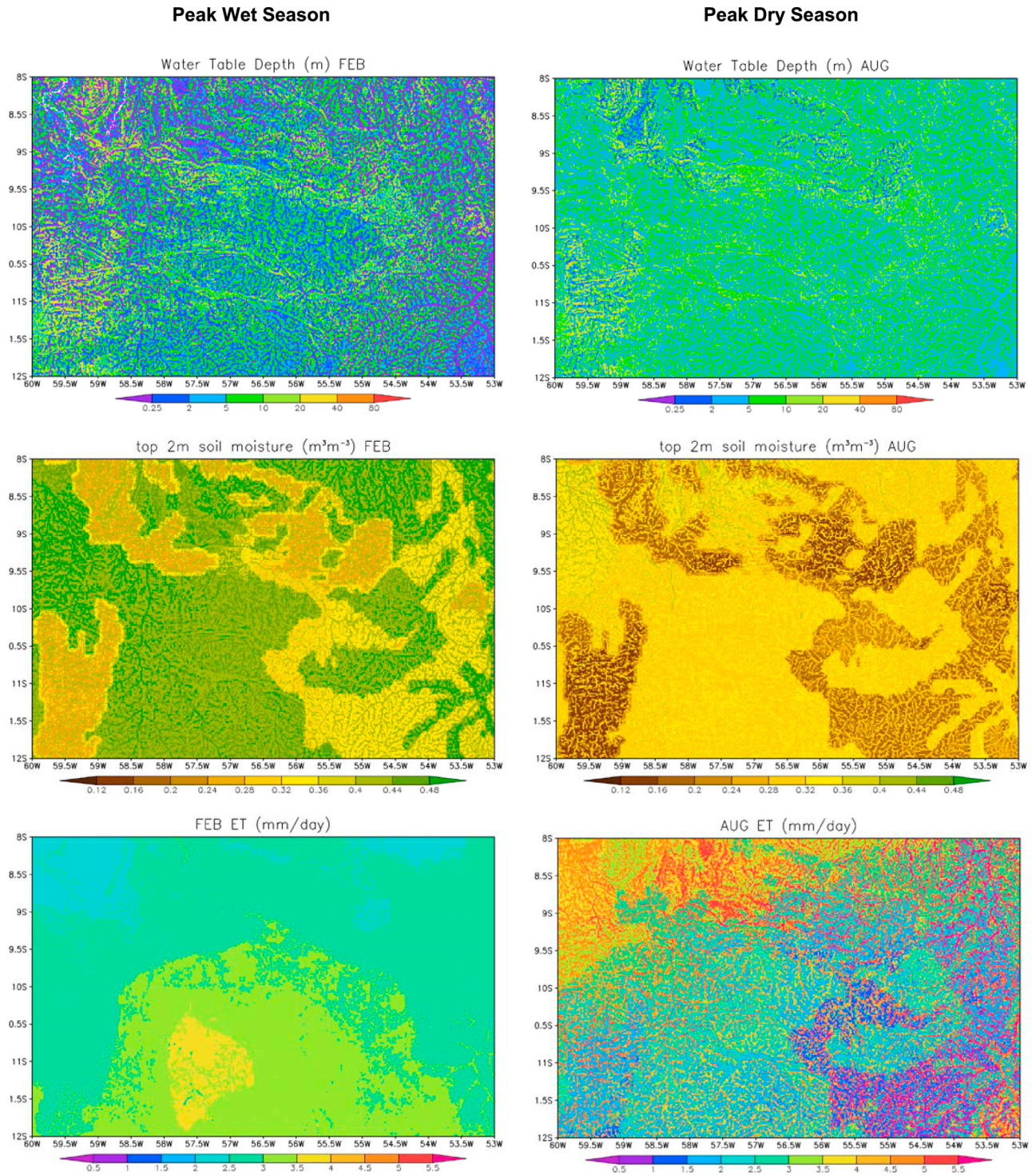

Figure 15. February and August water table depth (top), top-2 m soil moisture, and ET flux over a 4 × 7 degree box in Tapajos (location in Figure 12), showing the temporally persistent spatial structure in land surface moisture states and fluxes induced by topography-driven groundwater convergence into the valleys.

moisture capacity and memory to cope with the shorter and less intense dry seasons here. In the northern part of the continent such as the Orinoco Basin, the presence of the groundwater made a substantial difference. The same can be said in the southern part of the Amazon. Over the 4 × 7 degree box shown in Figure 12 and discussed in Figures 13–15, where the rainfall forcing and soil texture bias is the least, the simulated monthly ET difference is <0.1 mm/d for

December–May, and 0.2, 0.9, 1.2, 0.6, 0.3, and 0.1 mm/d for June–November, respectively, with the largest values in July (0.9) and August (1.2), the peak dry season. It is likely that allowing deeper roots and hydraulic redistribution (HR) can further enhance the divergence, the synergy of which with the groundwater will be investigated in a future study.

[58] We note that our results are based on model simulations, which only suggest the potential importance of the groundwater system to the Amazon water cycle. The ultimate knowledge must come from carefully designed field observations linking the vegetation, soil and groundwater, from water balance and tracer tests, and across a wide range of physical-biological settings. On the modeling side, adequate spatial data support, such as refined soil information both laterally and in greater depths, local pedo-transfer functions such as discussed in *Tomasella et al.* [2000], and better constrained atmospheric forcing data, are among the key issues that must be addressed in order to improve the realism of large-scale hydrologic models.

[59] We conclude that the groundwater reservoir may be an important regulator of the Amazon water cycle, which may have potential implications for understanding the Amazon carbon balance. The role of the Amazon ecosystem in the global carbon cycle as a net source or sink depends on the difference between the photosynthetic carbon uptake by forests and aquatic plants (the in-flux) and carbon export through respiration, aquatic outgassing and fluvial transport into the ocean (the out-flux). As suggested by the results here, the Amazon groundwater may regulate soil water stress on plant photosynthesis particularly in the dry season, and hence groundwater may be relevant to the carbon in-flux. As suggested by the results in the companion paper, groundwater can regulate the partition between surface runoff and deep infiltration, the former mobilizing soil and litter organic carbon and the latter dissolving and outgassing respired soil carbon, and groundwater can also maintain wetlands that are methane sources, and hence groundwater may also be relevant to the carbon out-fluxes. Our preliminary model results from the two companion papers suggest that the role of the groundwater may warrant further investigations, in both field and modeling studies. Finally, to illustrate the model simulated co-evolution of soil water and groundwater stores, an animation is provided as auxiliary material (Animation S1)[1] that portrays the changes of plant-available soil moisture in the top 2 m of land surface over 2001–2005 at 10 day-intervals, synchronized with changes in the water table depth.[1] This coupled evolution among the soil and groundwater stores is the norm in nature and needs to be represented in our models.

[60] **Acknowledgments.** Financial support comes from Ministerio de Educación y Ciencia de España (Spanish Ministry of Education and Science) CGL2006–13828, NSF-AGS-1045110, and EPA-STAR-RD834190. Computational support was provided by CESGA (Centro de Supercomputación de Galicia) Supercomputer Center at the Universidade de Santiago de Compostela, Galicia, Spain. We thank each and every LBA (http://daac.ornl.gov/LBA/lba.shtml) scientist who toiled in the field and obtained observations and analyses which have shed much light on the nature of the Amazon water cycle and provided data for evaluating our model; the list of names is simply too long to be shown here. The LBA project is funded by NASA, the Brazilian Ministry of Science and Technology and European Agencies. We also thank the LBA-Data-Model-Intercomparison project funded by NASA's Terrestrial Ecology Program (grant NNX09AL52G) which provided the data sets that made this work possible. We also thank Luis Gustavo G. de Gonçalves and Natalia Restrepo-Coupe for providing the LBA atmospheric data for evaluating the Interim forcing (Figure 5) through our participation in the LBA-Data-Model-Intercomparison project.

[1]Auxiliary materials are available in the HTML. doi:10.1029/2012JD017540.

References

Adler, R. F., et al. (2003), The version 2 Global Precipitation Climatology Project (GPCP) monthly precipitation analysis (1979–present), *J. Hydrometeorol.*, *4*, 1147–1167, doi:10.1175/1525-7541(2003)004<1147:TVGPCP>2.0.CO;2.

Amenu, G. G., and P. Kumar (2008), A model for hydraulic redistribution incorporating coupled soil-root moisture transport, *Hydrol. Earth Syst. Sci.*, *12*, 55–74, doi:10.5194/hess-12-55-2008.

Baker, I. T., L. Prihodko, A. S. Denning, M. Goulden, S. Miller, and H. R. da Rocha (2008), Seasonal drought stress in the Amazon: Reconciling models and observations, *J. Geophys. Res.*, *113*, G00B01, doi:10.1029/2007JG000644.

Balsamo, G., P. Viterbo, A. Beljaars, B. van den Hurk, M. Hirschi, A. K. Betts, and K. Scipal (2009), A revised hydrology for the ECMWF model: Verification from field site to terrestrial water storage and impact in the Integrated Forecast System, *J. Hydrometeorol.*, *10*, 623–643, doi:10.1175/2008JHM1068.1.

Bates, P. D., M. S. Horritt, and T. J. Fewtrell (2010), A simple inertial formulation of the shallow water equations for efficient two-dimensional flood inundation modeling, *J. Hydrol.*, *387*, 33–45, doi:10.1016/j.jhydrol.2010.03.027.

Beighley, R. E., K. G. Eggert, T. Dunne, Y. He, V. Gummadi, and K. L. Verdin (2009), Simulating hydrologic and hydraulic processes throughout the Amazon River Basin, *Hydrol. Processes*, *23*, 1221–1235, doi:10.1002/hyp.7252.

Betts, A. K., M. Kohler, and Y. Zhang (2009), Comparison of river basin hydrometeorology in ERA-Interim and ERA-40 reanalyses with observations, *J. Geophys. Res.*, *114*, D02101, doi:10.1029/2008JD010761.

Bongers, F., D. Engelen, and H. Klinge (1985), Phytomass structure of natural plant communities on spodosols in southern Venezuela: The Bana woodland, *Vegetatio*, *63*, 13–34, doi:10.1007/BF00032183.

Bonnet, M. P., et al. (2008), Floodplain hydrology in an Amazon floodplain lake (Lago Grande de Curuaı), *J. Hydrol.*, *349*, 18–30, doi:10.1016/j.jhydrol.2007.10.055.

Borma, L. S., et al. (2009), Atmosphere and hydrologic controls of the evapotranspiration over a floodplain forest in the Bananal Island region, Amazonia, *J. Geophys. Res.*, *114*, G01003, doi:10.1029/2007JG000641.

Bourrel, L., L. Phillips, and S. Moreau (2009), The dynamics of floods in the Bolivian Amazon Basin, *Hydrol. Processes*, *23*, 3161–3167, doi:10.1002/hyp.7384.

Bruno, R. D., H. R. da Rocha, D. C. de Freitas, M. L. Goulden, and S. D. Miller (2006), Soil moisture dynamics in an eastern Amazonian tropical forest, *Hydrol. Processes*, *20*, 2477–2489, doi:10.1002/hyp.6211.

Burgess, S. S. O., M. A. Adams, N. C. Turner, and C. K. Ong (1998), The redistribution of soil water by tree root systems, *Oecologia*, *115*, 306–311, doi:10.1007/s004420050521.

Caldwell, M. M., T. E. Dawson, and J. H. Richards (1998), Hydraulic lift: Consequences of water efflux from the roots of plants, *Oecologia*, *113*, 151–161, doi:10.1007/s004420050363.

Canadell, J., R. B. Jackson, J. R. Ehleringer, H. A. Mooney, O. E. Sala, and E. D. Schulze (1996), Maximum rooting depth of vegetation types at the global scale, *Oecologia*, *108*, 583–595, doi:10.1007/BF00329030.

Clapp, R. B., and G. M. Hornberger (1978), Empirical equations for some soil hydraulic properties, *Water Resour. Res.*, *14*, 601–604, doi:10.1029/WR014i004p00601.

Clapperton, C. (1993), *Quaternary Geology and Geomorphology of South America*, Elsevier, Amsterdam.

Coe, M. T., M. H. Costa, and E. A. Howard (2008), Simulating the surface waters of the Amazon River basin: Impacts of new river geomorphic and flow parameterizations, *Hydrol. Processes*, *22*, 2542–2553, doi:10.1002/hyp.6850.

Coomes, D. A., and P. J. Grubb (1996), Amazonian caatinga and related communities at La Esmeralda, Venezuela: Forest structure, physiognomy and floristics, and control by soil factors, *Vegetatio*, *122*, 167–191, doi:10.1007/BF00044699.

Cuartas, L. A. (2008), Estudo Observacional E De Modelagem Hidrologica De Uma Micro-Bacia Em Floresta Nao Perturbada Na Amazonia Central, PhD thesis, Inst. Nac. de Pesqui. Espaciais, Sao Jose dos Campos, Brazil.

Cullmann, J., W. J. Junk, G. Weber, and G. H. Schmitz (2006), The impact of seepage influx on cation content of a Central Amazonian floodplain lake, *J. Hydrol.*, *328*, 297–305, doi:10.1016/j.jhydrol.2005.12.027.

Czikowsky, M. J., and D. Fitzjarrald (2009), Detecting rainfall interception in an Amazonian rainforest with eddy flux measurements, *J. Hydrol.*, *377*, 92–105, doi:10.1016/j.jhydrol.2009.08.002.

da Rocha, H. R., M. Goulden, S. Miller, M. Menton, L. Pinto, H. Freitas, and A. S. Figueira (2004), Seasonality of water and heat fluxes over a tropical forest in eastern Amazonia, *Ecol. Appl.*, *14*(4), 22–32, doi:10.1890/02-6001.

da Rocha, H. R., et al. (2009), Patterns of water and heat flux across a biome gradient from tropical forest to savanna in Brazil, *J. Geophys. Res.*, *114*, G00B12, doi:10.1029/2007JG000640.

Dawson, T. E. (1993), Hydraulic lift and water use by plants: Implications for water balance, performance and plant-plant interactions, *Oecologia*, *95*, 565–574.

de Goncalves, L. G. G., et al. (2009), The South American Land Data Assimilation System (SALDAS) 5-yr retrospective atmospheric forcing datasets, *J. Hydrometeorol.*, *10*, 999–1010, doi:10.1175/2009JHM1049.1.

Dickinson, R. E., A. Henderson-Sellers, P. J. Kennedy, and M. F. Wilson (1986), Biosphere- atmosphere transfer scheme for the NCAR community climate model, *NCAR Tech. Note NCAR/TN-275+STR*, 69 pp., Natl. Cent. for Atmos. Res., Boulder, Colo.

Dingman, S. L. (2002), *Physical Hydrology*, 2nd ed., 600 pp., Prentice Hall, Upper Saddle River, N J.

Do Nascimento, N. R., E. Fritsch, G. T. Bueno, M. Bardy, C. Grimaldi, and A. J. Melfi (2008), Podzolization as a deferralitization process: Dynamics and chemistry of ground and surface waters in an Acrisol–Podzol sequence of the upper Amazon Basin, *Eur. J. Soil Sci.*, *59*, 911–924, doi:10.1111/j.1365-2389.2008.01049.x.

Eltahir, E. A. B., and R. L. Bras (1993), Estimation of the fractional coverage of rainfall in climate models, *J. Clim.*, *6*, 639–644, doi:10.1175/1520-0442(1993)006<0639:EOTFCO>2.0.CO;2.

Eltahir, E., and P. J.-F. Yeh (1999), On the asymmetric response of aquifer water level to floods and droughts in Illinois, *Water Resour. Res.*, *35*, 1199–1217, doi:10.1029/1998WR900071.

Eva, H. D., A. S. Belward, E. E. de Miranda, C. M. di Bella, V. Gonds, O. Huber, S. Jones, M. Sgrenzaroli, and S. Fritz (2004), A land cover map of South America, *Global Change Biol.*, *10*, 1–14, doi:10.1111/j.1529-8817.2003.00774.x.

Fan, Y., and G. Miguez-Macho (2010), Potential groundwater contribution to Amazon dry-season evapotranspiration, *Hydrol. Earth Syst. Sci.*, *14*, 2039–2056, doi:10.5194/hess-14-2039-2010.

Fisher J. A., et al. (2009), The land-atmosphere water flux in the tropics, *Global Change Biol.*, *15*, 2694–2714, doi:10.1111/j.1365-2486.2008.01813.x.

Forsberg, B. R., A. H. Devol, J. E. Richey, L. A. Martinelli, and H. dos Sandos (1988), Factors controlling nutrient concentrations in Amazon floodplain lakes, *Limnol. Oceanogr.*, *33*, 41–56, doi:10.4319/lo.1988.33.1.0041.

Freeze, R. A., and J. A. Cherry (1979), *Groundwater*, 604 pp., Prentice Hall, Upper Saddle River, N. J.

Germer, S., C. Neill, A. V. Krusche, and H. Elsenbeer (2010), Influence of land-use change on near-surface hydrological processes: Undisturbed forest to pasture, *J. Hydrol.*, *380*, 473–480, doi:10.1016/j.jhydrol.2009.11.022.

Good, P., C. Jones, J. Lowe, R. Betts, and B. Booth (2011), Quantifying environmental drivers of future tropical forest extent, *J. Clim.*, *24*, 1337–1349, doi:10.1175/2010JCLI3865.1.

Goulden, M., S. Miller, H. Rocha, M. Menton, and H. Freitas (2004), Physiological controls on tropical forest CO_2 exchange, *Ecol. Appl.*, *14*(4), 42–54, doi:10.1890/02-6008.

Grant, R. F., L. R. Hutyra, R. C. Oliveira, J. W. Munger, S. R. Saleska, and S. C. Wofsy (2009), Modeling the carbon balance of Amazonian rain forests: Resolving ecological controls on net ecosystem productivity, *Ecol. Monogr.*, *79*(3), 445–463, doi:10.1890/08-0074.1.

Grogan, J., and J. Galvão (2006), Physiographic and floristic gradients across topography in transitional seasonally dry evergreen forests of southeast Para, Brazil, *Acta Amazon.*, *36*, 483–496, doi:10.1590/S0044-59672006000400009.

Grubb, P. J. (1977), Control of forest growth and distribution on wet tropical mountains: With special reference to mineral nutrition, *Annu. Rev. Ecol. Syst.*, *8*, 83–107, doi:10.1146/annurev.es.08.110177.000503.

Hamilton, S. K., J. Kellndorfer, B. Lehner, and M. Tobler (2007), Remote sensing of floodplain geomorphology as a surrogate for biodiversity in a tropical river system (Madre de Dios, Peru), *Geomorphology*, *89*, 23–38, doi:10.1016/j.geomorph.2006.07.024.

Harper, A. B., A. S. Denning, I. T. Baker, M. D. Branson, L. Prihodko, and D. A. Randall (2010), Role of deep soil moisture in modulating climate in the Amazon rainforest, *Geophys. Res. Lett.*, *37*, L05802, doi:10.1029/2009GL042302.

Hess, L. L., J. M. Melack, E. M. L. M. Novo, C. C. F. Barbosa, and M. Gastil (2003), Dual-season mapping of wetland inundation and vegetation for the central Amazon basin, *Remote Sens. Environ.*, *87*, 404–428, doi:10.1016/j.rse.2003.04.001.

Hess, L. L., J. M. Melack, E. M. L. M. Novo, C. C. F. Barbosa, and M. Gastil (2009), LBA-ECO LC-07 Central Amazon Wetlands 100 m Mask based on JERS SAR Images (v.0), http://www.daac.ornl.gov, Oak Ridge Natl. Lab., Oak Ridge, Tenn.

Hodnett, M. G., I. Vendrame, A. D. O. Margues Filho, M. D. Oyama, and J. Tomasella (1997a), Soil water storage and groundwater behaviour in a catenary sequence beneath forest in central Amazonia. I. Comparisons between plateau, slope and valley floor, *Hydrol. Earth Syst. Sci.*, *1*, 265–277, doi:10.5194/hess-1-265-1997.

Hodnett, M. G., I. Vendrame, A. D. O. Margues Filho, M. D. Oyama, and J. Tomasella (1997b), Soil water storage and groundwater behaviour in a catenary sequence beneath forest in central Amazonia. II. Floodplain water table behaviour and implications for streamflow generation, *Hydrol. Earth Syst. Sci.*, *1*, 279–290, doi:10.5194/hess-1-279-1997.

Huete, A. R., K. Didan, Y. Z. Shimabukuro, P. Ratana, S. R. Saleska, L. R. Hutyra, W. Yang, R. R. Nemani, and R. Myneni (2006), Amazon rainforests green-up with sunlight in dry season, *Geophys. Res. Lett.*, *33*, L06405, doi:10.1029/2005GL025583.

Ichii, K., H. Hashimoto, M. A. White, C. Potter, L. R. Hutyra, A. R. Huete, R. B. Myneni, and R. R. Nemani (2007), Constraining rooting depths in tropical rainforests using satellite data and ecosystem modeling for accurate simulation of gross primary production seasonality, *Global Change Biol.*, *13*, 67–77, doi:10.1111/j.1365-2486.2006.01277.x.

Jirka, S., A. J. McDonald, M. S. Johnson, T. R. Feldpausch, E. G. Couto, and S. J. Riha (2007), Relationships between soil hydrology and forest structure and composition in the southern Brazilian Amazon, *J. Veg. Sci.*, *18*, 183–194, doi:10.1111/j.1654-1103.2007.tb02529.x.

Johnson, M. S., J. Lehmann, E. C. Selva, M. Abdo, S. Riha, and E. G. Couto (2006), Organic carbon fluxes within and streamwater exports from headwater catchments in the southern Amazon, *Hydrol. Processes*, *20*, 2599–2614, doi:10.1002/hyp.6218.

Juárez, R. I. N., M. G. Hodnett, R. Fu, M. Goulden, and C. von Randow (2007), Control of dry season evapotranspiration over the Amazonian forest as inferred from observations at a southern Amazon forest site, *J. Clim.*, *20*, 2827–2839, doi:10.1175/JCLI4184.1.

Keller, M., M. Bustamante, J. Gash, and P. Silva Bias (Eds.) (2009), *Amazonia and Global Change*, *Geophys. Monogr. Ser.*, vol. 186, 565 pp., AGU, Washington, D. C., doi:10.1029/GM186.

Kleidon, A., and M. Heimann (2000), Assessing the role of deep rooted vegetation in the climate system with model simulations: Mechanism, comparison to observations and implications for Amazonian deforestation, *Clim. Dyn.*, *16*, 183–199, doi:10.1007/s003820050012.

Lähteenoja, O., and S. Page (2011), High diversity of tropical peatland ecosystem types in the Pastaza-Marañón basin, Peruvian Amazonia, *J. Geophys. Res.*, *116*, G02025, doi:10.1029/2010JG001508.

Lawrence, D. M., P. H. Thornton, K. W. Oleson, and G. B. Bonan (2007), The partitioning of evapotranspiration into transpiration, soil evaporation, and canopy evaporation in a GCM: Impacts on land-atmosphere interaction, *J. Hydrometeorol.*, *8*, 862–880, doi:10.1175/JHM596.1.

Lee, J.-E., R. S. Oliveira, T. Dawson, and I. Fung (2005), Root functioning modifies seasonal climate, *Proc. Natl. Acad. Sci. U. S. A.*, *102*, 17,576–17,581.

Lesack, L. F. W. (1995), Seepage exchange in an Amazon floodplain lake, *Limnol. Oceanogr.*, *40*, 598–609, doi:10.4319/lo.1995.40.3.0598.

Lesack, L. F. W., and J. M. Melack (1995), Flooding hydrology and mixture dynamics of lake water derived from multiple sources in an Amazon floodplain lake, *Water Resour. Res.*, *31*, 329–345, doi:10.1029/94WR02271.

Lo, M.-H., and J. S. Famiglietti (2010), Effect of water table dynamics on land surface hydrologic memory, *J. Geophys. Res.*, *115*, D22118, doi:10.1029/2010JD014191.

Lo, M.-H., and J. S. Famiglietti (2011), Precipitation response to land subsurface hydrologic processes in atmospheric general circulation model simulations, *J. Geophys. Res.*, *116*, D05107, doi:10.1029/2010JD015134.

Malhi, Y., L. E. O. C. Aragao, D. Galbraith, C. Huntingford, R. Fisher, P. Zelazowski, S. Sitch, C. McSweeney, and P. Meir (2009), Exploring the likelihood and mechanism of a climate-change-induced dieback of the Amazon rainforest, *Proc. Natl. Acad. Sci. U. S. A.*, *106*, 20,610–20,615, doi:10.1073/pnas.0804619106.

Marengo, J. A., J. Tomasella, L. M. Alves, W. R. Soares, and D. A. Rodriguez (2011), The drought of 2010 in the context of historical droughts in the Amazon region, *Geophys. Res. Lett.*, *38*, L12703, doi:10.1029/2011GL047436.

Maritan, A., A. Rinaldo, R. Rigon, A. Giacometti, and I. Rodríguez-Iturbe (1996), Scaling laws for river networks, *Phys. Rev. E*, *53*, 1510–1515, doi:10.1103/PhysRevE.53.1510.

Markewitz, D., S. Devine, E. A. Davidson, P. Brando, and D. C. Nepstad (2010), Soil moisture depletion under simulated drought in the Amazon: Impacts on deep root uptake, *New Phytol.*, *187*, 592–607, doi:10.1111/j.1469-8137.2010.03391.x.

McClain, M. E., J. E. Richey, and J. A. Brandes (1997), Dissolved organic matter and terrestrial-lotic linkages in the central Amazon basin of Brazil, *Global Biogeochem. Cycles*, *11*, 295–311, doi:10.1029/97GB01056.

Meade, R. H., J. M. Rayol, S. C. da Conceicao, and J. R. G. Natividate (1991), Backwater effects in the Amazon River Basin of Brazil, *Environ. Geol. Water Sci.*, *18*(2), 105–114, doi:10.1007/BF01704664.

Mertes, L. A. K. (1997), Documentation and significance of the perirheic zone on inundated floodplains, *Water Resour. Res.*, *33*, 1749–1762, doi:10.1029/97WR00658.

Miguez-Macho, G., and Y. Fan (2012), The role of groundwater in the Amazon water cycle: 1. Influence on seasonal streamflow, flooding and wetlands, *J. Geophys. Res.*, *117*, D15113, doi:10.1029/2012JD017539.

Miguez-Macho, G., Y. Fan, C. P. Weaver, R. Walko, and A. Robock (2007), Incorporating water table dynamics in climate modeling: 2. Formulation, validation, and soil moisture simulation, *J. Geophys. Res.*, *112*, D13108, doi:10.1029/2006JD008112.

Moreira, M. Z., L. S. L. Sternberg, and D. C. Nepstad (2000), Vertical patterns of soil water uptake by plants in a primary forest and an abandoned pasture in the eastern Amazon: An isotopic approach, *Plant Soil*, *222*, 95–107, doi:10.1023/A:1004773217189.

Myneni, R. B., et al. (2007), Large seasonal swings in leaf area of Amazon rainforests, *Proc. Natl. Acad. Sci. U. S. A.*, *104*, 4820–4823, doi:10.1073/pnas.0611338104.

Nepstad, D. C., C. R. de Carvalho, E. A. Davidson, P. H. Jipp, P. A. Lefebvre, G. H. Negreiros, E. D. da Silva, T. A. Stone, S. E. Trumbore, and S. Vieira (1994), The role of deep roots in the hydrological and carbon cycles of Amazonian forests and pastures, *Nature*, *372*, 666–669, doi:10.1038/372666a0.

Neu, V., C. Neill, and A. V. Krusche (2011), Gaseous and fluvial carbon export from an Amazon forest watershed, *Biogeochemistry*, *105*, 133–147, doi:10.1007/s10533-011-9581-3.

Niu, G.-Y., Z. L. Yang, R. E. Dickinson, L. E. Gulden, and H. Su (2007), Development of a simple groundwater model for use in climate models and evaluation with Gravity Recovery and Climate Experiment data, *J. Geophys. Res.*, *112*, D07103, doi:10.1029/2006JD007522.

Niu, G.-Y., et al. (2011), The community Noah land surface model with multiparameterization options (Noah-MP): 1. Model description and evaluation with local-scale measurements, *J. Geophys. Res.*, *116*, D12109, doi:10.1029/2010JD015139.

Oliveira, R. S., T. E. Dawson, S. S. O. Burgess, and D. C. Nepstad (2005), Hydraulic redistribution in three Amazonian trees, *Oecologia*, *145*, 354–363, doi:10.1007/s00442-005-0108-2.

Pelletier, J. D., and C. Rasmussen (2009), Geomorphically based predictive mapping of soil thickness in upland watersheds, *Water Resour. Res.*, *45*, W09417, doi:10.1029/2008WR007319.

Poels, R. L. H. (1987), *Soils, Water and Nutrients in a Forest Ecosystem in Suriname*, Agric. Univ. at Wageningen, Wageningen, Netherlands.

Poulter, B., F. Hattermann, E. Hawkins, S. Zaehles, S. Sitch, A. Restrepo-Coupe, U. Heyder, and W. Cramer (2010), Robust dynamics of Amazon dieback to climate change with perturbed ecosystem model parameters, *Global Change Biol.*, *16*, 2476–2495, doi:10.1111/j.1365-2486.2009.02157.x.

Prance, G. T. (1987), Soils and vegetation, in *Biogeography and Quaternary History in Tropical America*, edited by T. C. Whitmore and G. T. Prance, pp. 19–45, Clarendon Press, Oxford, U. K.

Press, W. H., B. P. Flannery, S. A. Teukolsky, and W. T. Vetterling (1989), *Numerical Recipes–The Art of Scientific Computing (FORTRAN Version)*, 702 pp., Cambridge Univ. Press, Cambridge, U. K.

Rinaldo, A., I. Rodríguez-Iturbe, R. Rigon, R. L. Bras, E. J. Ijjasz-Vasquez, and A. Marani (1992), Minimum energy and fractal structures of drainage networks, *Water Resour. Res.*, *28*, 2183–2195, doi:10.1029/92WR00801.

Rodríguez-Iturbe, I., E. J. Ijjász-Vásquez, R. L. Bras, and D. G. Tarboton (1992), Power law distribution of discharge mass and energy in river basins, *Water Resour. Res.*, *28*, 1089–1093, doi:10.1029/91WR03033.

Romero-Saltos, H. L., L. S. L. Sternberg, M. Z. Moreira, and D. C. Nepstad (2005), Rainfall exclusion in an eastern Amazonian forest alters soil water movement and depth to water uptake, *Am. J. Bot.*, *92*, 443–455, doi:10.3732/ajb.92.3.443.

Sakaguchi, K., and X. Zeng (2009), Effects of soil wetness, plant litter, and under-canopy atmospheric stability on ground evaporation in the Community Land Model (CLM3.5), *J. Geophys. Res.*, *114*, D01107, doi:10.1029/2008JD010834.

Sakaguchi, K., X. Zeng, B. J. Christoffersen, N. Restrepo-Coupe, S. R. Saleska, and P. M. Brando (2011), Natural and drought scenarios in an east central Amazon forest: Fidelity of the Community Land Model 3.5 with three biogeochemical models, *J. Geophys. Res.*, *116*, G01029, doi:10.1029/2010JG001477.

Saleska, S. R., et al. (2003), Carbon in Amazon Forests: Unexpected seasonal fluxes and disturbance-induced losses, *Science*, *302*, 1554–1557, doi:10.1126/science.1091165.

Saleska, S., H. da Rocha, B. Kruijt, and A. Nobre (2009), Ecosystem carbon fluxes and Amazonian forest metabolism, in *Amazonia and Global Change*, *Geophys. Monogr. Ser.*, vol. 186, edited by M. Keller et al., pp. 389–407, AGU, Washington, D. C., doi:10.1029/2008GM000728.

Schenk, H. J., and R. B. Jackson (2002), The global biogeography of roots, *Ecol. Monogr.*, *72*, 311–328, doi:10.1890/0012-9615(2002)072[0311:TGBOR]2.0.CO;2.

Schulze, E.-D., et al. (1996), Rooting depth, water availability, and vegetation cover along an aridity gradient in Patagonia, *Oecologia*, *108*, 503–511, doi:10.1007/BF00333727.

Selhorst, D., S. A. Vieira, and I. F. Brown (2003), Agua e crescimento de uma floresta na Amazonia Sul-Ocidental, Acre, Brasil: Chuva afeta crescimento, mas nıvel do lencol freatico nao, poster report, Univ. Fed. do Acre, Rio Branco, Brazil. [ftp://lba.cptec.inpe.br/lba_archives/LC/LC-02/Posters/SelhorstDiogo_Poster_VI_CEB_02nov03.pdf.]

Sellers, P. J., D. A. Randall, G. J. Collatz, J. A. Berry, C. B. Field, D. A. Dazlich, C. Zhang, G. D. Collelo, and L. Bounoua (1996a), A revised land surface parameterization (SiB2) for atmospheric GCMs. Part I: Model formulation, *J. Clim.*, *9*, 676–705, doi:10.1175/1520-0442(1996)009<0676:ARLSPF>2.0.CO;2.

Sellers, P. J., S. O. Los, C. J. Tucker, C. O. Justice, D. A. Dazlich, G. J. Collatz, and D. A. Randall (1996b), A revised land surface parameterization (SiB2) for atmospheric GCMs. Part II: The generation of global fields of terrestrial biophysical parameters from satellite data, *J. Clim.*, *9*, 706–737, doi:10.1175/1520-0442(1996)009<0706:ARLSPF>2.0.CO;2.

Shuttleworth, W. J. (1988), Evaporation from Amazonian rainforest, *Proc. R. Soc. London, Ser. B*, *233*, 321–346, doi:10.1098/rspb.1988.0024.

Sternberg, L. S. L., M. Z. Moreira, and D. C. Nepstad (2002), Uptake of water by lateral roots of small trees in an Amazonian tropical forest, *Plant Soil*, *238*, 151–158, doi:10.1023/A:1014214404699.

Thornton, P. E., and N. Zimmerman (2007), An improved canopy integration scheme for a land surface model with prognostic canopy structure, *J. Clim.*, *20*, 3902–3923, doi:10.1175/JCLI4222.1.

Tomasella, J., M. G. Hodnett, and L. Rossato (2000), Pedotransfer function for the estimation of soil water retention in Brazilian soils, *Soil Sci. Soc. Am. J.*, *64*, 327–338, doi:10.2136/sssaj2000.641327x.

Tomasella, J., M. G. Hodnett, L. A. Cuartas, A. D. Nobre, M. J. Waterloo, and S. M. Oliveira (2008), The water balance of an Amazonian microcatchment: The effect of interannual variability of rainfall on hydrological behavior, *Hydrol. Processes*, *22*, 2133–2147, doi:10.1002/hyp.6813.

Trigg, M. A., M. D. Wilson, P. D. Bates, M. S. Horritt, D. E. Alsdor, B. R. Forsbert, and M. C. Vega (2009), Amazon flood wave hydraulics, *J. Hydrol.*, *374*, 92–105, doi:10.1016/j.jhydrol.2009.06.004.

Verbeeck, H., P. Peylin, C. Bacour, D. Bonal, K. Steppe, and P. Ciais (2011), Seasonal patterns of CO_2 fluxes in Amazon forests: Fusion of eddy covariance data and the ORCHIDEE model, *J. Geophys. Res.*, *116*, G02018, doi:10.1029/2010JG001544.

Vourlitis, G. L., J. D. Nogueira, F. D. Lobo, K. M. Sendall, S. R. de Paulo, C. A. A. Dias, O. B. Pinto Jr., and N. L. R. de Andrade (2008), Energy balance and canopy conductance of a tropical semi-deciduous forest of the southern Amazon Basin, *Water Resour. Res.*, *44*, W03412, doi:10.1029/2006WR005526.

Walko, R. L., and C. J. Tremback (2005), Modifications from the transition from LEAF-2 to LEAF-3, *ATMET Tech. Note 1*, Atmos. Meteorol. and Environ. Technol., Boulder, Colo. [Available at http://www.atmet.com/html/docs/rams/RT1-leaf2-3.pdf.]

Walko, R. L., et al. (2000), Coupled atmosphere-biophysics-hydrology models for environmental modeling, *J. Appl. Meteorol.*, *39*, 931–944, doi:10.1175/1520-0450(2000)039<0931:CABHMF>2.0.CO;2.

Wang, D., G. Wang, and E. N. Anagnostou (2007), Evalution of canopy interception schemes in land surface models, *J. Hydrol.*, *347*, 308–318, doi:10.1016/j.jhydrol.2007.09.041.

Wang, G. (2011), Assessing the potential hydrological impacts of hydraulic redistribution in Amazonia using a numerical modeling approach, *Water Resour. Res.*, *47*, W02528, doi:10.1029/2010WR009601.

Wang, G. L., and E. A. B. Eltahir (2000), Impact of rainfall subgrid variability on modeling the biosphere atmosphere system, *J. Clim.*, *13*, 2887–2899, doi:10.1175/1520-0442(2000)013<2887:MTBAST>2.0.CO;2.

Werth, D., and R. Avissar (2004), The regional evapotranspiration of the Amazon, *J. Hydrometeorol.*, *5*, 100–109, doi:10.1175/1525-7541(2004)005<0100:TREOTA>2.0.CO;2.

Winter, T. C., J. W. Harvey, O. L. Franke, and W. A. Alley (1998), Ground water and surface water: A single resource, *U.S. Geol. Surv. Circ.*, *1139*, 79 pp.

Xiao, X., Q. Zhang, S. Saleska, L. Hutyra, P. De Camargo, S. Wofsy, S. Frolking, S. Boles, M. Keller, and B. Moore (2005), Satellite-based modeling of gross primary production in a seasonally moist tropical evergreen forest, *Remote Sens. Environ.*, *94*, 105–122, doi:10.1016/j.rse.2004.08.015.

Yamazaki, D., S. Kanae, H. Kim, and T. Oki (2011), A physically based description of floodplain inundation dynamics in a global river routing model, *Water Resour. Res.*, *47*, W04501, doi:10.1029/2010WR009726.

Yang, Z.-L., et al. (2011), The community Noah land surface model with multi-parameterization options (Noah-MP): 2. Evaluation over global river basins, *J. Geophys. Res.*, *116*, D12110, doi:10.1029/2010JD015140.

Zelazowski, P., Y. Malhi, C. Huntingford, S. Sitch, and J. Fisher (2011), Changes in the potential distribution of humid tropical forests on a warmer planet, *Philos. Trans. R. Soc. A*, *369*, 137–160, doi:10.1098/rsta.2010.0238.